



HAL
open science

Impact of membrane lipid polyunsaturation on dopamine D2 receptor ligand binding and signaling

Marie-Lise Jobin, Véronique de Smedt-Peyrusse, Fabien Ducrocq, Asma Oummadi, Rim Baccouch, Maria Hauge Pedersen, Brian Medel-Lacruz, Pierre van Delft, Laetitia Fouillen, Sébastien Mongrand, et al.

► To cite this version:

Marie-Lise Jobin, Véronique de Smedt-Peyrusse, Fabien Ducrocq, Asma Oummadi, Rim Baccouch, et al.. Impact of membrane lipid polyunsaturation on dopamine D2 receptor ligand binding and signaling. 2023. hal-04286162v1

HAL Id: hal-04286162

<https://hal.science/hal-04286162v1>

Preprint submitted on 28 Oct 2022 (v1), last revised 15 Nov 2023 (v2)

HAL is a multi-disciplinary open access archive for the deposit and dissemination of scientific research documents, whether they are published or not. The documents may come from teaching and research institutions in France or abroad, or from public or private research centers.

L'archive ouverte pluridisciplinaire **HAL**, est destinée au dépôt et à la diffusion de documents scientifiques de niveau recherche, publiés ou non, émanant des établissements d'enseignement et de recherche français ou étrangers, des laboratoires publics ou privés.

1 **Impact of membrane lipid polyunsaturation on dopamine D2 receptor ligand binding**
2 **and signaling**

3 Marie-Lise Jobin^{1*}, Véronique De Smedt-Peyrusse^{1*}, Fabien Ducrocq¹, Asma Oummadi¹,
4 Rim Baccouch², Maria Hauge Pedersen^{3,4}, Brian Medel-Lacruz⁵, Pierre Van Delft⁶, Laetitia
5 Fouillen⁶, Sébastien Mongrand⁶, Jana Selent⁵, Tarson Tolentino-Cortez⁷, Gabriel Barreda-
6 Gómez⁷, Stéphane Grégoire⁸, Elodie Masson⁸, Thierry Durroux⁹, Jonathan A. Javitch^{3,4,10},
7 Ramon Guixà-González^{11,12*}, Isabel D. Alves^{2*}, Pierre Trifilieff^{1*}

8
9 ¹ Université de Bordeaux, INRAE, Bordeaux INP, NutriNeuro, 33000, Bordeaux, France

10 ² Institute of Chemistry & Biology of Membranes & Nanoobjects, CNRS UMR 5248,
11 Université de Bordeaux, Bordeaux INP, 33600 Pessac, France

12 ³ Department of Psychiatry, Columbia University Vagelos College of Physicians and
13 Surgeons, New York, NY 10032

14 ⁴ Division of Molecular Therapeutics, New York State Psychiatric Institute, New York, NY
15 10032

16 ⁵ Research Programme on Biomedical Informatics (GRIB), Hospital del Mar Medical
17 Research Institute (IMIM)—Department of Experimental and Health Sciences, Pompeu
18 Fabra University (UPF), 08003 Barcelona, Spain

19 ⁶ Laboratory of Membrane Biogenesis (LBM), Research Mix Unity (UMR) 5200, National
20 Scientific Research Center (CNRS), University of Bordeaux, Bordeaux, France

21 ⁷ Research Department, IMG Pharma Biotech S.L., BIC Bizkaia (612), 48160 Derio, Spain

22 ⁸ Centre des Sciences du Goût et de l'Alimentation, AgroSup Dijon, CNRS, INRAE,
23 Université Bourgogne Franche-Comté, 21000 Dijon, France

24 ⁹ Institut de Génomique Fonctionnelle, CNRS, INSERM, Université de Montpellier,
25 Montpellier, France

26 ¹⁰ Department of Molecular Pharmacology and Therapeutics, Columbia University Vagelos
27 College of Physicians and Surgeons, New York, NY 10032

28 ¹¹ Laboratory of Biomolecular Research, Paul Scherrer Institute (PSI), 5232 Villigen PSI,
29 Switzerland

30 ¹² Condensed Matter Theory Group, PSI, 5232 Villigen PSI, Switzerland

40 **Abstract**

41 The heterogenous and dynamic constitution of the membrane fine-tunes signal transduction.
42 In particular, the polyunsaturated fatty acid (PUFA) tails of phospholipids influence the
43 biophysical properties of the membrane, production of second messengers, or membrane
44 partitioning. Few evidence mostly originating from studies of rhodopsin suggest that PUFAs
45 directly modulate the conformational dynamic of transmembrane proteins. However, whether
46 such properties translate to other G protein-coupled receptors remains unclear. We focused
47 on the dopamine D2 receptor (D2R), a main target of antipsychotics. Membrane enrichment in
48 n-3, but not n-6, PUFAs potentiates ligand binding. Molecular dynamics simulations show that
49 the D2R preferentially interacts with n-3 over n-6 PUFAs. Furthermore, even though this mildly
50 affects signalling in heterologous systems, *in vivo* n-3 PUFA deficiency blunts the effects of
51 D2R ligands. These results suggest that n-3 PUFAs act as allosteric modulators of the D2R
52 and provide a putative mechanism for their potentiating effect on antipsychotic efficacy.

53

54 **Introduction**

55 Biological membranes are not homogeneous bilayers but rather composed of different lipid
56 species with various chemical and biophysical properties that actively modulate protein
57 localization and function, signaling or vesicular trafficking ¹. However, several aspects of
58 membrane complexity including the impact of lipid heterogeneity across tissues, cells, and
59 subcellular compartments on cell signaling and physiology are only starting to emerge.

60

61 This is particularly true for neuronal function for which the impact of membrane lipid
62 composition has been largely overlooked, despite that the brain has the second highest lipid
63 content after adipose tissue ². Yet, convergent findings support some links between lipid
64 biostatus and mental health. For instance, a decrease in the levels of n-3 polyunsaturated fatty
65 acids (PUFAs)-containing phospholipids has been consistently described in a subset of
66 patients suffering from neurodevelopmental psychiatric diseases ³. Likewise, recent
67 transcriptomic profiling studies revealed a common pattern in fatty acid metabolic pathways in
68 several psychiatric disorders ^{4,5}. Moreover, n-3 PUFA deficiency in rodent models has been
69 associated with putative pathophysiological mechanisms involving alteration in neurogenesis,
70 neuronal migration, neuromodulation, and neuroinflammatory processes in various brain
71 regions ^{2,6,7}. These findings remain largely correlative and the precise mechanisms by which
72 PUFA biostatus directly or indirectly accounts for changes in neuronal function remain largely
73 unknown. Nevertheless, several studies have demonstrated that membrane lipids regulate the
74 function of key transmembrane proteins ⁸ including ion channels and GPCRs ^{9,10}.

75

76 The activity of the dopamine D2 receptor (D2R) is particularly relevant in this context. Various
77 psychiatric disorders, including those where levels of brain n-3 PUFAs are low ¹¹, display
78 altered patterns of D2R-dependent signaling, and this GPCR is, therefore, a key target in
79 several pharmacological treatments. Similarly, different studies in rodent models show that n-
80 3 PUFA deficiency affects dopamine transmission and related behaviors ^{12,13}. In line with this
81 evidence, we recently reported a unique vulnerability of D2R-expressing neurons to PUFA
82 biostatus that directly accounts for the motivational deficits induced by n-3 PUFA deficiency ¹⁴.
83 Early experimental studies have reported that n-3 PUFAs, namely docosahexaenoic acid
84 (DHA, 22:6), enhance the function of the prototypical A GPCR rhodopsin ¹⁵⁻¹⁷. Subsequent
85 studies showed that DHA-containing phospholipids preferentially solvate rhodopsin ^{18,19}, which
86 could impact receptor function. In addition, recent *in silico* studies ^{20,21} demonstrate that the
87 D2R also displays a preference for DHA interaction that could modulate receptor partitioning
88 into specific membrane signaling platforms, as shown by early experiments ²². While these

89 findings suggest that membrane PUFA composition could influence the activity of the D2R,
90 there is still no direct evidence of such an effect.

91

92 In this work, using both cell membrane extracts and model membranes, we found that DHA,
93 but not n-6 PUFA docosapentaenoic acid (DPA, 22:5), enhances D2R ligand binding affinity.
94 Strikingly, while DPA and DHA only differ in one double bond, molecular dynamics (MD)
95 simulations show that they have a completely different propensity for interaction with the D2R.
96 Interestingly, membrane enrichment in either DHA or DPA have no effect on agonist-induced,
97 $G_{i/o}$ protein-dependent inhibition of cAMP production. However, both DHA and DPA similarly
98 enhance the maximal efficacy of the D2R to recruit β -arrestin2 upon agonist stimulation.
99 Finally, we provide *in vivo* evidence that DHA deficiency blunts the behavioral effects of D2R
100 ligands. Altogether, these data highlight the impact of membrane PUFA composition on D2R
101 activity and suggest that DHA acts as an allosteric modulator of the receptor.

102

103 **Results**

104

105 **1. Membrane n-3 PUFAs, but not n-6 PUFAs, modulate the binding affinity of D2R** 106 **ligands**

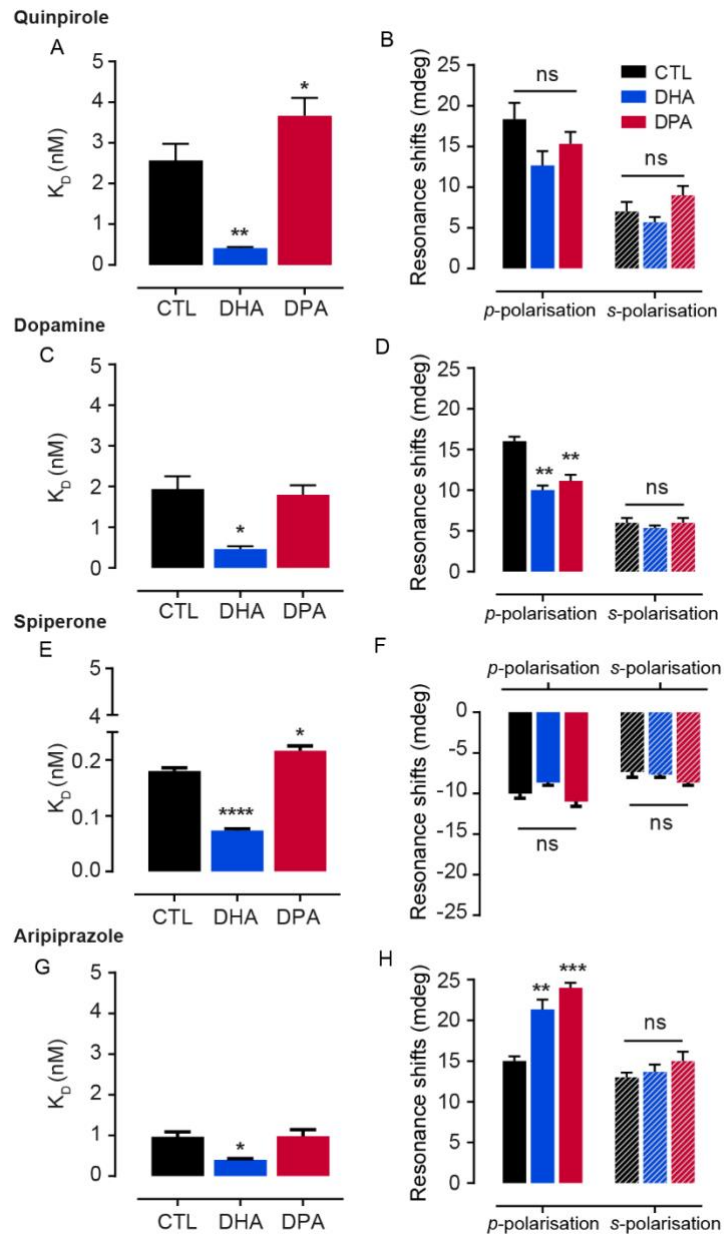
107 To determine the impact of membrane lipid unsaturation on D2R ligand binding, HEK cells
108 were incubated with PUFAs, which is known to result in their esterification in *sn*-2 position of
109 phospholipids²³. We used two different PUFAs, the n-3 PUFA DHA (C22:6) and the n-6 PUFA
110 DPA (C22:5), which display the same carbon chain length, but differ in one double bond. A
111 lipid analysis confirmed the enrichment of phospholipids in DHA or DPA and monitored its
112 efficient incorporation in cell membranes, leading to comparable proportion of either PUFA
113 after treatment (increase of 19% for DHA and 20% for DPA) (Fig. S1). We measured the
114 binding affinity of D2R ligands on supported cell membranes expressing the D2R using
115 plasmon waveguide resonance (PWR) spectroscopy²⁴. The resonance position shifts were
116 followed in *p*- (perpendicular to the sensor surface) and *s*-polarisation (parallel to the sensor
117 surface) upon poly-L-Lysine (PLL) coating of the PWR sensor and subsequent cell membrane
118 adhesion and detachment (Fig. S2A and B). The cell membrane fragment deposition led to
119 positive shifts similar to those observed for synthetic lipid bilayer formation²⁵. We measured
120 the resonance shifts upon incremental addition of ligand when the time curve reached a
121 plateau (Fig. S2C and D) and led to shifts in the minimum resonance. These cumulative shifts
122 were plotted as a binding curve which allowed calculating a dissociation constant (K_D) and

123 measuring a plateau of the resonance shifts (Fig. S3). The K_D calculated for the agonist
124 quinpirole and the antagonist spiperone were comparable to the ones reported in the literature,
125 validating our system and confirming that the receptor maintains functionality in these
126 conditions (Fig. S3C)^{26,27}. The results from these experiments show that membrane DHA
127 enrichment enhances ligand binding affinities for agonists (quinpirole and dopamine),
128 antagonist (spiperone), and partial agonist (aripiprazole) (Fig. 1). However, DPA slightly
129 decreased D2R binding affinity for quinpirole and spiperone (Fig. 1A and E) and had no effect
130 for dopamine and aripiprazole (Fig. 1C and G). We further confirmed the potentiating effect of
131 membrane DHA enrichment on D2R ligand binding affinity for the spiperone-derived
132 fluorescent ligand NAPS-d2 through fluorescence anisotropy^{28,29} (Fig. S4) and in partially
133 purified D2R reconstituted in model membranes (Fig. S5).

134

135 To study ligand-induced receptor conformational changes, we quantified the direction and
136 magnitude of minimum resonance in *p*- and *s*-polarizations, which account for changes along
137 the receptor long and short axis, respectively. Resonance shifts obtained upon ligand addition
138 were positive in both polarisations for agonists (quinpirole, dopamine) and partial agonist
139 (aripiprazole), and negative for the antagonist spiperone (Fig. 1F). These results show that
140 different classes of ligands induce distinct conformational changes upon binding to the D2R,
141 as previously reported for other GPCRs^{30–34}. While the presence of membrane PUFAs did not
142 significantly influence the changes in conformation induced by quinpirole and spiperone (Fig.
143 1B and F), they impacted the conformation of dopamine- and aripiprazole-bound D2Rs
144 regarding the anisotropy of the conformational state that became less anisotropic for dopamine
145 and more anisotropic for aripiprazole (as shown by the respective decrease and increase in *p*-
146 polarization shifts; Figs. 1D and 1H).

147



148

149 **Figure 1. D2R binding affinity in PUFA-enriched cell membranes shown by PWR.** PUFA effect on
150 binding affinity and receptor conformational changes, respectively, for quinpirole (A and B), dopamine
151 (C and D), spiperone (E and F) and aripiprazole (G and H). Data are mean \pm SEM values from 3
152 independent experiments with **** $p < 0.0001$, *** $p < 0.001$, ** $p < 0.01$, * $p < 0.05$ by two-tailed unpaired t-
153 test.

154 **2. MD simulations reveal that n-3 and n-6 PUFAs differentially interact with the**
 155 **D2R**

156
 157 With the aim of gaining structural insights into the differential modulation exerted by DPA and
 158 DHA in PUFA-enriched cell membranes, we used MD simulations to study the interaction
 159 between the D2R and membranes enriched in either DHA or DPA. We first simulated four
 160 replicas of the D2R embedded in a multicomponent membrane (see Methods) enriched in
 161 either DHA-containing phospholipids (1-stearoyl-2-docosahexaenoyl-sn-glycero-3-
 162 phosphocholine, SD(h)PC) or DPA-containing phospholipids (1-stearoyl-2-
 163 docosa(p)entaenoyl-sn-glycero-3-phosphocholine, SD(p)PC). In line with previous reports,
 164 ^{20,21} SD(h)PC tends to displace saturated phospholipids from the membrane “solvation” shell
 165 that surrounds the D2R, due to the much higher propensity of DHA tails for the interaction with
 166 the receptor (Fig. 2A). Strikingly, the loss of just one double bond (i.e. replacing DHA by DPA)
 167 is enough to abolish this propensity, as shown by the much lower interaction ratio of SD(p)PC
 168 molecules with the receptor during the simulation (Fig. 2B). Specifically, the propensity for the
 169 interaction with the D2R is three-fold higher for DHA tails (Table 1).

170

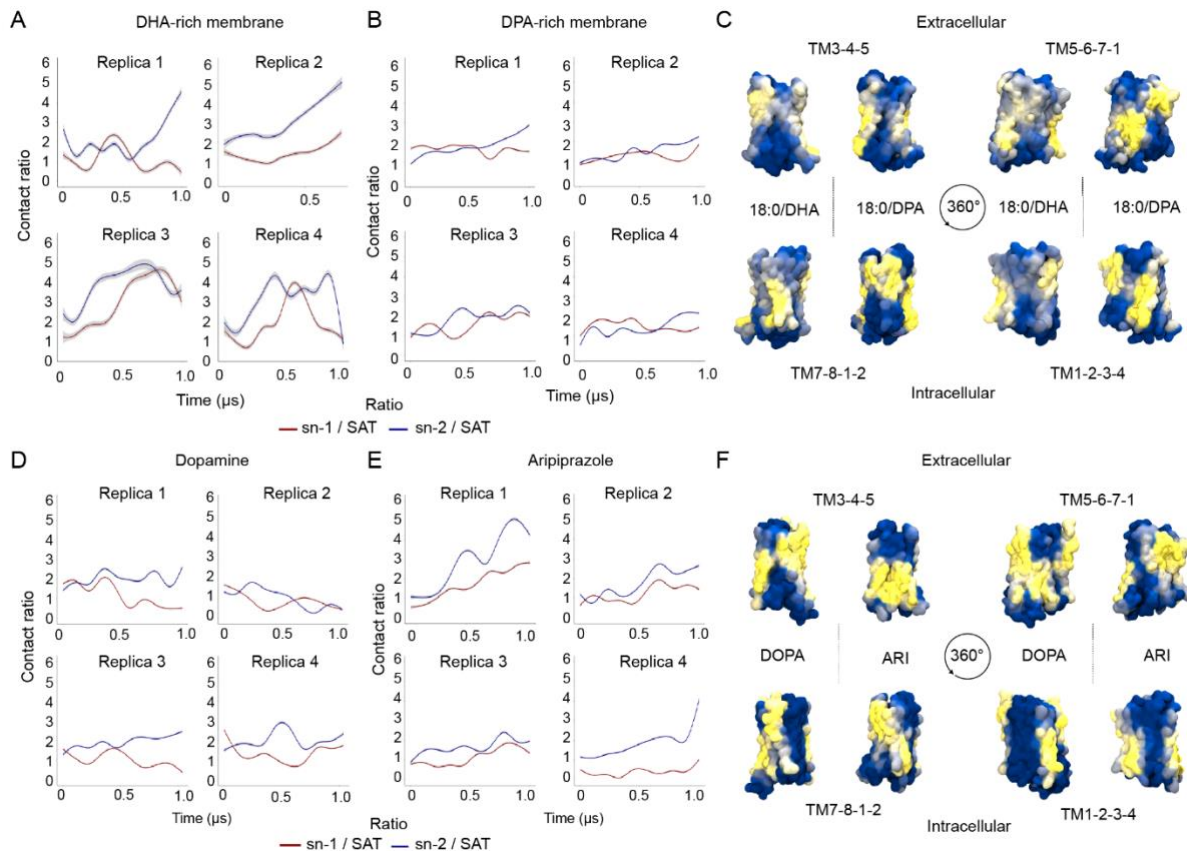
Ratio	0 - 250 ns	250 - 500 ns	500 – 750 ns	750 ns - 1 μ s
SD(h)PC _{sn-1}	0.97	1.69	2.95	2.42
SD(h)PC_{sn-2} (DHA)	2.01	3.05	4.61	4.08
SD(p)PC _{sn-1}	1.49	1.48	1.48	1.63
SD(p)PC_{sn-2} (DPA)	1.47	1.95	2.28	2.33

171 **Table 1. Evolution of lipid-protein contacts during MD simulations.** The table shows the average
 172 relative proportion of lipid-protein contacts at four stages of the simulation. Contact ratios represent the
 173 number of atomic contacts between each SD(h)PC or SD(p)PC chain (i.e. sn-1 or sn-2) and the D2R,
 174 with respect to the number of contacts between saturated phospholipids (i.e. DPPC, DSPC, and PSM)
 175 and the protein (see Methods for more details).

176

177 From these results, it is reasonable to speculate that the more flexible lipid corona built around
 178 the D2R in DHA-rich membranes could allow for greater dynamics within the receptor, which
 179 could potentially enhance protein conformational selection during the ligand binding process.
 180 This scenario would accord with our ligand binding experiments, where DHA-rich membranes
 181 consistently induced lower K_{Ds} , i.e. higher binding affinities, than DPA-rich membranes (Fig.
 182 1). Moreover, our simulations show that despite DHA and DPA only differing in one double
 183 bond, they display a different pattern of interaction with the receptor (Fig. 2C). Some of these
 184 differences could also impact ligand binding affinity at the D2R. For example, SD(p)PC lipid
 185 molecules display a clear preference over SD(h)PC for interaction with the extracellular
 186 segments of transmembrane helix (TM) 1, TM2, and TM7, which are known to define entry

187 crevices for water and phospholipid headgroups into the binding pocket³⁵ (Fig. 2C, bottom
 188 left).
 189
 190



191

192 **Figure 2. Lipid-protein contacts during MD simulations. (A, B, D, E)** Relative proportion of atomic
 193 lipid-protein contacts (y-axis) over time (x-axis) for the simulations of the apo state of the D2R embedded
 194 in DHA- (A) versus DPA-rich (B) membranes, and the simulations of dopamine- (D) versus aripiprazole-
 195 bound D2R (E) embedded in DHA-rich membranes. Specifically, figures depict the contact ratio of each
 196 SD(h)PC or SD(p)PC chain versus all saturated lipids (i.e. DPPC, DSPC, and PSM) in the system (i.e.
 197 sn-1 / SAT and sn-2 / SAT) is depicted (see Methods for a detail description of these ratios). (C, F)
 198 Average lipid occupancy map for the simulations of the apo state of the D2R embedded in DPA- versus
 199 DHA-containing phospholipids (C), and the simulations of dopamine- (DOPA) versus aripiprazole (ARI)-
 200 bound D2R embedded in DHA-rich membranes (F). The percentage of frames where SD(h)PC or
 201 SD(p)PC lipid molecules contacted the D2R is depicted in a blue (low) to yellow (high) color gradient
 202 mapped to the surface of the receptor.
 203

204 We also simulated the D2R bound to dopamine or aripiprazole molecules, and embedded into
 205 a multicomponent membrane enriched in SD(h)PC (see Methods). Interestingly, while the
 206 aripiprazole-bound D2R simulations also showed an increased level of DHA around the
 207 receptor (Fig. 2E), the DHA solvation effect was absent or even diminished in dopamine-bound
 208 D2R simulations (Fig. 2D). Specifically, the propensity for the interaction between DHA tails
 209 and the protein was approximately two-fold higher in the aripiprazole-bound D2R simulations
 210 (Table 2).
 211

	Ratio	0 - 250 ns	250 - 500 ns	500 - 750 ns	750 ns - 1 μ s
DOPA	SD(h)PC _{sn-1}	1.16	0.98	1.00	0.81
	SD(h)PC_{sn-2} (DHA)	1.78	1.63	1.62	1.73
ARI	SD(p)PC _{sn-1}	0.97	1.46	1-65	1.67
	SD(p)PC_{sn-2} (DHA)	1.75	2.87	3.12	3.07

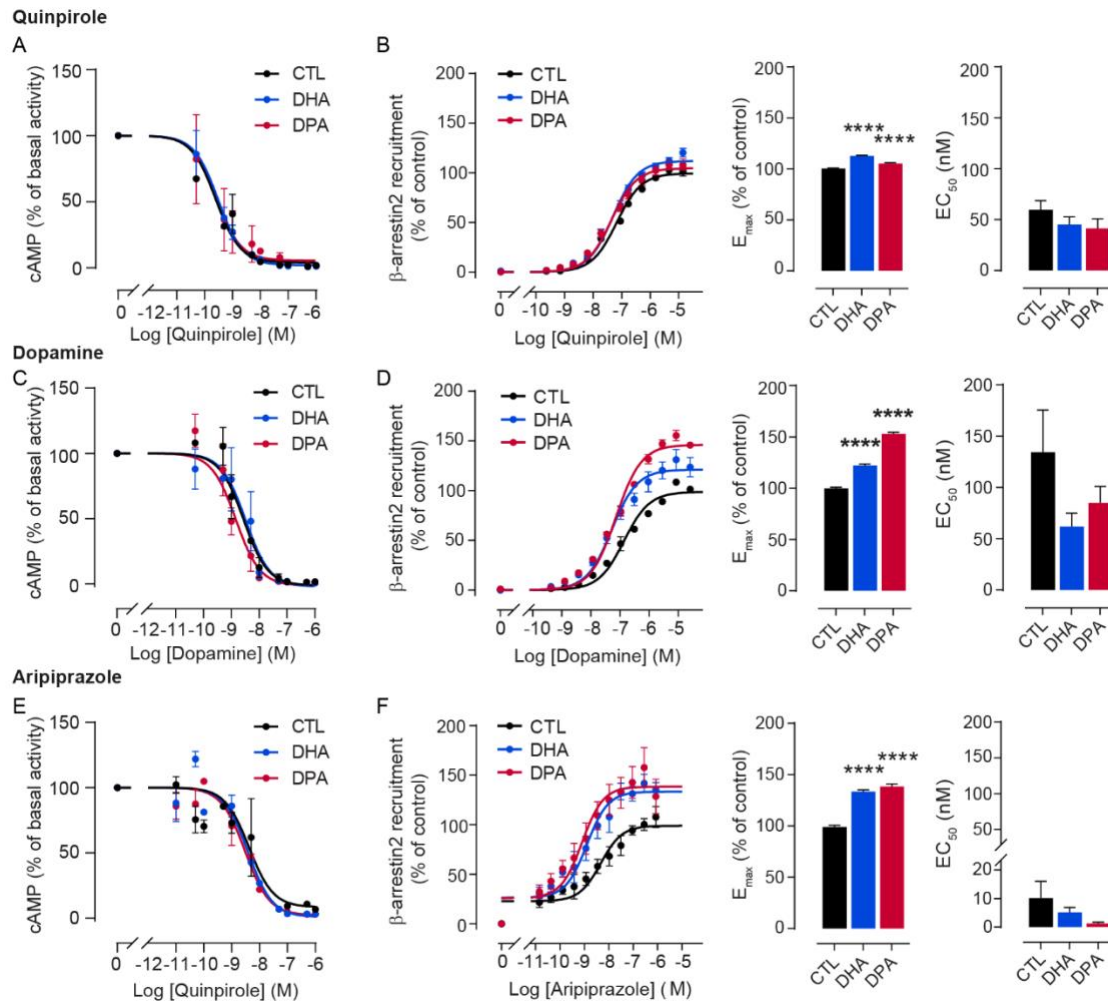
212 **Table 2. Evolution of lipid-protein contacts during ligand-bound D2R simulations.** The table shows
 213 the average relative proportion of lipid-protein contacts at four stages of the simulation. Contact ratios
 214 represent the number of atomic contacts between each SD(h)PC chain (i.e. sn-1 or sn-2) and the
 215 dopamine (DOPA)- or aripiprazole (ARI)-bound D2R, with respect to all saturated lipids (i.e. DPPC,
 216 DSPC and PSM) (see Methods for exact membrane composition and details on the calculation of these
 217 ratios).
 218

219 Furthermore, as shown in Fig. 2F, the presence of the ligand in the binding pocket induced a
 220 different pattern of interactions between SD(h)PC and the D2R, including a different interaction
 221 signature at the extracellular segment of the receptor where ligand binds (Fig. 2F, upper left
 222 and right panels)
 223

224 3. n-3 and n-6 PUFAs do not influence the D₂R G_{αi/o}-mediated signaling pathway but 225 enhance maximal recruitment of β-arrestin2 226

227 In order to evaluate the downstream effect of PUFAs, we performed dose-response
 228 experiments where we probed the signaling efficacy of the D2R in the presence and absence
 229 of PUFAs. First, we treated cells with 10 μ M PUFAs (Fig. S6) and measured the inhibition of
 230 forskolin-induced cAMP production upon quinpirole, dopamine and aripiprazole binding as a
 231 proxy for G_{i/o} protein signaling. As shown in Fig. S7A and Table S1, both control and PUFA-
 232 rich cells display a similar agonist-dependent decrease in cAMP production, which suggests
 233 that PUFAs do not modulate the G_{i/o} protein signaling pathway. Next, we used the same
 234 experimental conditions to study the G_{i/o} protein-independent signaling pathway by measuring
 235 β-arrestin2 recruitment. In these experiments, while PUFAs did not affect the potency of β-
 236 arrestin2 recruitment (i.e. EC₅₀), they either substantially (aripiprazole) or slightly (quinpirole
 237 and dopamine) affected its efficacy (i.e. E_{max}) (Fig. S7C, S7D, S7E). To confirm this trend, we
 238 treated cells with a higher amount of PUFAs (i.e. 30 μ M) (Fig. S6) and we did not observe any
 239 impact of PUFAs enrichment on basal cAMP production (Fig. S7B). We then performed dose-
 240 response experiments upon ligand stimulation. Higher PUFA manipulations did not influence
 241 cAMP production or the EC₅₀ for β-arrestin2 recruitment (Figs. 3A, 3C, and 3E), but significantly
 242 increased the E_{max} of β-arrestin2 recruitment for all ligands in both DHA- and DPA-rich cells
 243 (Figs. 3B, 3D, and 3F).

244 Altogether, our data reveal that both DPA and DHA exert a similar effect on downstream
 245 signaling, namely they do not affect $G_{i/o}$ protein activation but they are able to enhance β -
 246 arrestin2 recruitment efficacy.
 247



248

249 **Figure 3. Forskolin-stimulated cAMP production and β -arrestin2 recruitment upon ligand**
 250 **stimulation and with different membrane PUFAs enrichment. (A, C, E) Dose-response experiments**
 251 **of cAMP production with the D2R ligands quinpirole (A), dopamine (C) and aripiprazole (E), on forskolin-**
 252 **stimulated cells incubated in the presence of 0.03% ethanol as control, 30 μ M DHA and 30 μ M DPA n-**
 253 **6. Values are expressed as the percentage of cAMP in the absence of agonist in n=3 independent**
 254 **experiments. (B, D, F) Quinpirole (B), Dopamine (D) and aripiprazole (F) activity on D2R mediated β -**
 255 **arrestin2 assay in CHO-K1 cells expressing the DRD2L (left panel), and associated E_{max} (middle) and**
 256 **EC_{50} (right panel) under 30 μ M PUFAs enrichment. Data are mean \pm SEM values from three**
 257 **independent experiments with **** p<0.0001, *** p<0.001, * p<0.05 by two-tailed unpaired t-test.**

258

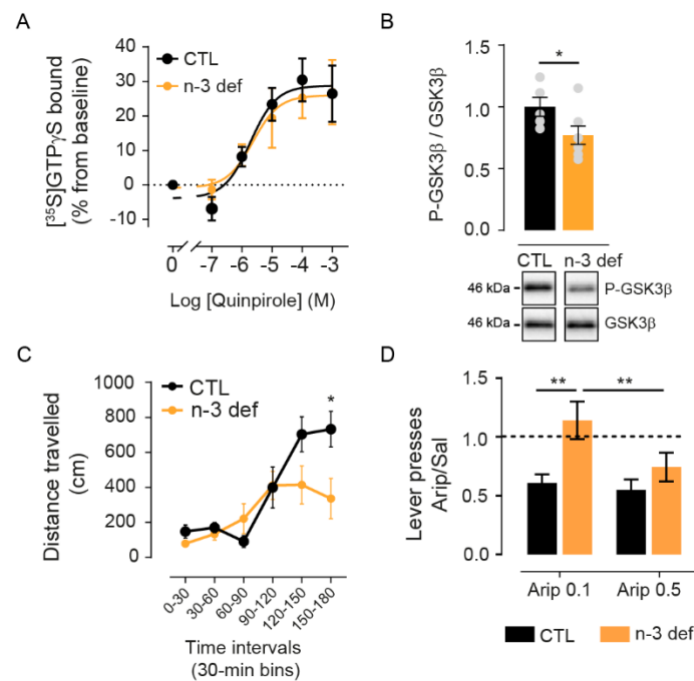
259 4. n-3 PUFA deficiency alters D2R ligand-induced alterations in locomotion and 260 motivation

261

262 To translate our *in vitro* findings to *in vivo* settings, we used a validated model of n-3 PUFA
 263 deficiency in mice. Using such an approach, we previously demonstrated that i) n-3 PUFA

264 deficiency leads to decreased and increased levels of DHA and DPA in membrane
265 phospholipids, respectively and ii) n-3 PUFA deficient animals display motivational deficits that
266 are due to impaired functionality of D2R-expressing neurons ¹⁴. Herein, using striatal extracts
267 – in which D2R is highly expressed – we found that i) Gi protein recruitment at the receptor
268 under quinpirole application is unaffected (Fig. 4A) and ii) phosphorylation of the glycogen
269 synthase kinase β (GSK3 β), a key signaling enzyme downstream of β -arrestin2 ³⁶, is
270 decreased at basal states in n-3 PUFA deficient animals (Fig. 4B and S8). These latter findings
271 are consistent with our in vitro data showing that membrane PUFA enrichment potentiates the
272 recruitment of β -arrestin2 at the D2R. Next, we used n-3 PUFA deficient animals to study
273 behavioral responses to D2R ligands. Our results show that n-3 PUFA deficient animals display
274 decreased locomotor response under quinpirole administration (Fig. 4C). Finally, we found that
275 peripheral administration of aripiprazole blunted performance in an operant conditioning-based
276 motivational task in control animals, while n-3 PUFA deficient mice were partially insensitive
277 to aripiprazole (Fig. 4D).
278

279



280

281 **Figure 4.** Effect of n-3 PUFA deficiency on D2R signalling and associated behaviors. **(A)** [³⁵S]GTP γ S
 282 assay on nucleus *accumbens* extracts upon increasing concentrations of quinpirole from control (CTL)
 283 or n-3 PUFA deficient animals (n-3 def). CTL : logEC50 = -5.22 \pm 0.28 %, Emax = 30.06 \pm 3.47 % ; n-3
 284 def : logEC50 = -5.06 \pm 0.29; Emax = 28.15 \pm 3.51 % **(B)** Western blots measuring the phosphorylation
 285 of GSK3 β (P-GSK3 β) relative to GSK3- β . Bars represent the mean of 5 and 7 subjects for CTL and n-3
 286 def respectively and error bars the SEM. *p<0.05 by Mann Whitney test. **(C)** Locomotor response to 1
 287 mg/kg quinpirole administration is represented as the distance travelled in cm divided in 30 min intervals
 288 in control (CTL, n=10) or n-3 def (n=10) animals. **(D)** Ratio of lever presses performed by animals under
 289 aripiprazole (0.1 or 0.5 mg/kg) over saline administration in a progressive ratio task in CTL (n=11) or n-
 290 3 def (n=10) animals. Data are mean \pm SEM values. ** p<0.01, * p<0.05 by two-way (RM) ANOVA test
 291 with a post-hoc Bonferroni test.

292 Discussion

293 While most early reports on the preferential interaction between PUFAs and GPCRs involved
294 n-3 PUFAs (i.e. DHA) and rhodopsin^{15–19}, recent studies have confirmed that DHA can also
295 modulate the activity and function of other GPCRs including the cannabinoid CB1 receptor³⁷,
296 the D2R^{20,21} and the adenosine A2A receptor^{20,21,38}. Here, we focus on D2R interplay with
297 PUFAs and show that (a) DHA- but not DPA-rich phospholipids potentiate the binding affinity
298 of both agonists and antagonists for the D2R; (b) both DPA and DHA enhance β -arrestin2
299 recruitment efficacy without affecting $G_{i/o}$ protein activity; and (c) n-3 deficient animal models
300 display altered behavioral responses upon treatment with D2R ligands.

301

302 PUFA-containing phospholipids can have a strong influence on the physical and mechanical
303 properties of biological membranes including thickness, bending or rigidity³⁹ and, hence,
304 subtle changes in these properties can indirectly modulate the function of transmembrane
305 proteins^{39–41}. Therefore, PUFA-rich membranes could potentially favor specific conformations
306 of the D2R to modulate its ligand binding affinity. In particular, n-3 PUFAs provide
307 transmembrane proteins with a uniquely flexible environment that enables such modulation^{41–}
308 ⁴³. Interestingly, despite differing in just one double bond, n-6 PUFAs do not seem to increase
309 membrane elasticity to the same extent⁴⁴. Furthermore, by increasing membrane fluidity
310 and/or packing defects⁸, PUFAs could change D2R accessibility for ligands thus modulating
311 their affinity. In fact, most antipsychotics (i.e. D2R ligands) display high membrane partitioning
312 properties^{45,46}. Of note, Lolicato et al. have recently shown that the entry pathway of dopamine
313 into the D2R likely requires this neurotransmitter to first partition into the membrane⁴⁷.

314

315 On the other hand, different studies demonstrate that PUFAs tend to preferentially interact with
316 GPCRs^{18,19,48,49}; thus, changes in ligand binding affinity could also be the result of direct
317 interactions between PUFAs and the D2R. In the current study, MD simulations confirm that
318 DHA tails preferentially interact with the D2R when compared to saturated ones, as previously
319 reported^{20,21}. Intriguingly, our simulations show that this preferential interaction is lower or
320 completely absent in the presence of aripiprazole or dopamine in the D2R binding pocket,
321 respectively. This result suggests a more complex scenario where the conformational state
322 induced by the ligand could also modulate the interaction propensity between the membrane
323 and the receptor, as recently suggested for cholesterol and the oxytocin receptor⁵⁰.
324 Interestingly, our simulations also show that n-6 PUFAs (i.e. DPA) have a much lower tendency
325 to interact with the receptor, despite DHA and DPA only differing in one double bond. While
326 further work is needed to unravel the precise molecular mechanisms behind the effect of DHA
327 on ligand binding affinity, our work suggests that DHA can act as an allosteric modulator of the

328 D2R, both by influencing the bulk membrane properties and by establishing direct interactions
329 with the receptor.

330

331 However, our dose-response experiments in cells show that the enhancing effect of PUFAs on
332 D2R ligand binding affinity does not correlate with an increased signal of relevant downstream
333 protein effectors. On the one hand, enriching membranes with PUFAs did not alter cAMP
334 production (i.e. $G_{i/o}$ protein signaling). This result is in line with different early^{51,52} and more
335 recent reports⁵³. On the other hand, PUFA-rich membranes do enhance the maximal efficacy
336 of β -arrestin2 recruitment, which seems to support a mechanism in which these lipids modulate
337 specific protein effectors. This is compatible with the fact that PUFAs can alter the lateral
338 organization of membranes^{23,54-56} or change the domain partitioning properties of GPCRs
339 including the D2R^{20,21}. Changes in the properties of membrane microdomains could also affect
340 the affinity of palmitoyl moieties for these domains, which could in turn affect receptor
341 partitioning. As previously suggested⁵⁷⁻⁶², altering receptor partitioning could indirectly
342 modulate receptor phosphorylation and, hence, influence β -arrestin coupling. It is also worth
343 speculating that PUFA-induced membrane packing defects⁸ could alter β -arrestin recruitment
344 by modulating the membrane anchoring of C-edge loops⁶³. Therefore, one plausible albeit
345 speculative hypothesis is that PUFAs could selectively modulate D2R signaling properties by
346 altering membrane lateral organization and/or influencing β -arrestin anchoring to the
347 membrane. It is worth noting that (a) the potency (EC50) of β -arrestin recruitment does not
348 change, and (b) both DPA and DHA exert comparable effects on protein signaling whereas
349 only DHA is capable of enhancing ligand binding. Altogether, these data suggest that the
350 effects of PUFAs on D2R signaling are at least partially uncoupled from the changes in receptor
351 binding properties. However, it should be noted that the relatively small changes in ligand
352 binding affinity induced by PUFAs on ligand binding affinity might be difficult to detect using
353 signalling assays in heterologous system. Nonetheless, such subtle modifications might have
354 important physiological impact in the context of chronic alterations in PUFA levels, in particular
355 when occurring during brain development.

356 This hypothesis is supported by our *in vivo* findings in a model of chronic deficiency in n-3
357 PUFAs¹⁴. In fact, in accordance with our *in vitro* results, while n-3 PUFA deficiency does not
358 seem to affect D2R binding of the $G_{i/o}$ protein in the striatum, the decrease in phospho-GSK3
359 expression is consistent with an impairment of β -arrestin2-dependent signaling, since GSK3
360 phosphorylation depends on β -arrestin2 recruitment at the D2R³⁶. Notably, D2R-mediated
361 locomotor response has recently been shown to also depend on β -arrestin2-, but not $G_{i/o}$
362 protein-, mediated signalling⁶⁴. In line with this, we find that D2R agonist (quinpirole)-induced
363 increase in locomotion is blunted in n-3 PUFA deficient animals, consistent with an impairment

364 in β -arrestin2 recruitment and downstream signalling. Yet, however, we find that aripiprazole-
365 induced decrease in motivation – which might result from an antagonistic activity of aripiprazole
366 at the D2R - is also blunted in n-3 PUFA deficient animals. D2R-mediated modulation of
367 motivation has been shown to be independent of β -arrestin2-dependent signalling⁶⁴, but rather
368 to rely on $G_{i/o}$ protein-mediated transmission at synaptic terminals in the ventral pallidum⁶⁵.
369 This raises the intriguing hypothesis that membrane PUFAs could differentially modulate D2R
370 signalling activity depending on neuronal subcompartments. Even though further work will be
371 needed to disentangle the precise mechanisms by which PUFAs modulate D2R activity *in vivo*,
372 these latter data are in line with the recent demonstration that motivational deficits in n-3 PUFA
373 deficient animals directly relates to a dysfunction of D2R-expressing neurons¹⁴.

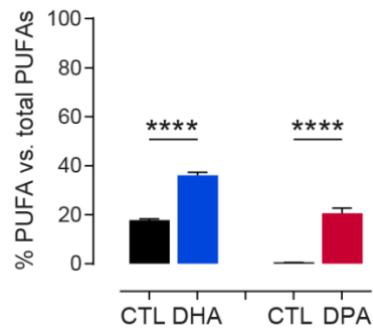
374

375 Unveiling the precise mechanisms by which brain PUFA biostatus impacts D2R-dependent
376 signaling and downstream-related behaviors will require further work. Nonetheless, taken
377 together, our results show that n-3 PUFAs could act as allosteric modulators of the D2R and
378 potentiate its signalling activity, in particular the β -arrestin2 component. This raises the
379 intriguing hypothesis that n-3 PUFA supplementation could allow potentiating the efficacy of
380 D2R ligands, several of them being antipsychotics. In accordance with this idea, several clinical
381 trials have shown that n-3 PUFA supplementation accelerates treatment response, improves
382 the tolerability of antipsychotics in first-episode psychoses^{66,67}, and reduces prescription rate
383 of antipsychotics⁶⁸. Our data suggest that direct action of PUFA membrane composition on
384 D2R activity could mediate such alleviating effects.

385

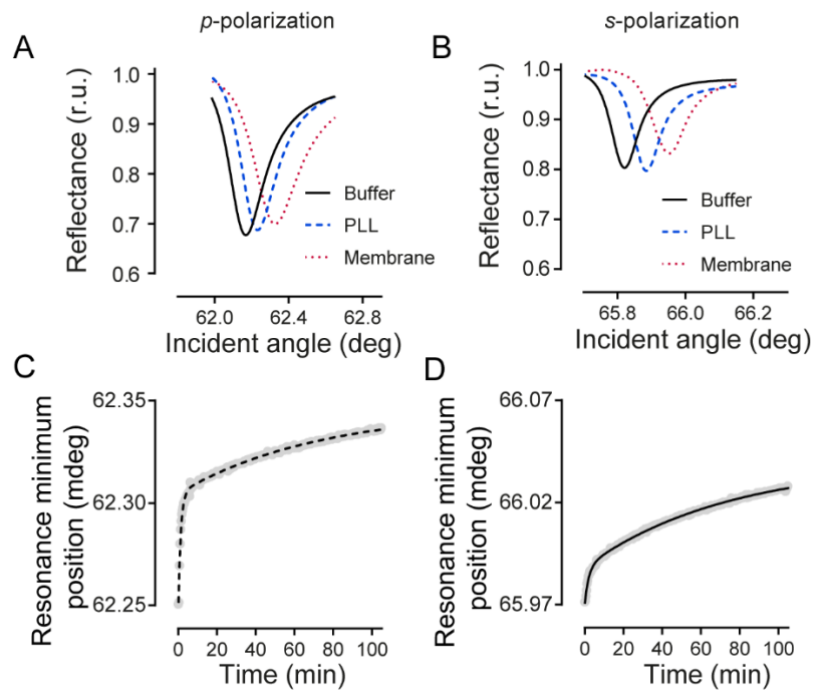
386 **Supplementary figures**

387



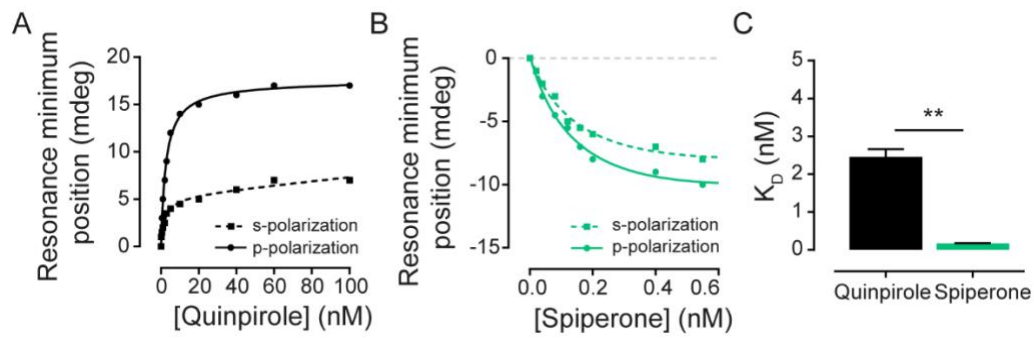
388

389 **Figure S1. PUFAs enrichment in HEK cells.** HEK cells were incubated with DHA or DPA at 10 μ M
390 concentration. Each PUFA enrichment is compared to control cells incubated with vehicle only (0.03 %
391 ethanol). Bars represent the mean average of three independent experiments and error bars represent
392 the standard error of the mean (SEM). **** $p < 0.0001$ by two-tailed unpaired t-test.



393

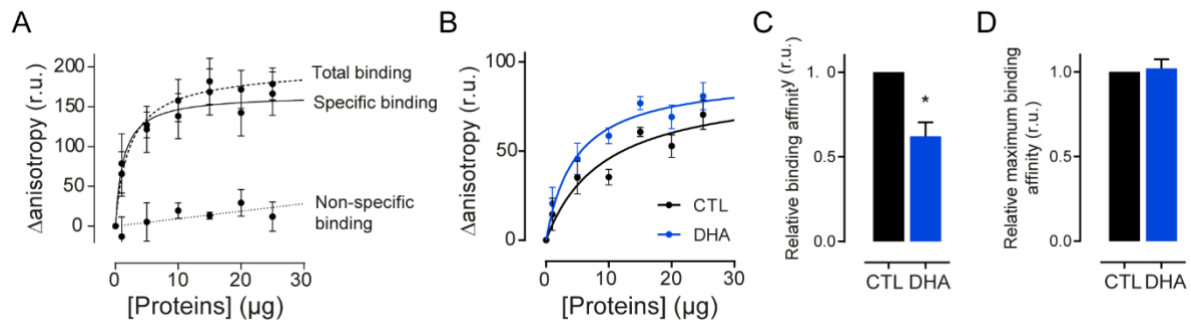
394 **Figure S2. Capture of cell membrane fragments on the PWR sensor and reconstitution of**
395 **detergent-solubilised D2R in a lipid model membrane.** Capture of cell membrane fragments
396 containing the D2R following PLL treatment of the PWR sensor followed by PWR using *p*- and *s*-
397 polarization. **(A and B)** Representative PWR spectra following sensor coating with polylysine (PLL; blue)
398 and cell membrane fragment capture (red) obtained with *p*- (A) and *s*- (B) polarized light, respectively.
399 **(C and D)** Kinetics of D2R reconstitution in a POPC lipid membrane observed for *p*- (C) and *s*-
400 polarizations (D). Kinetics were fitted to a two-phase exponential growth.
401



402

403 **Figure S3. Agonist and antagonist binding with D2R present in cell membranes monitored by**
404 **PWR.** Quinpirole (A) and spiperone (B) were incrementally added to the proteolipid membrane and the
405 shifts in the resonance minimum position followed. The data were fitted with a hyperbolic binding
406 equation that describes total binding to a single site in the receptor (more details in Materials and
407 Methods). (C) Affinity binding of quinpirole and spiperone calculated from (A) and (B) respectively. ** p
408 < 0.01 by two-tailed unpaired t-test.

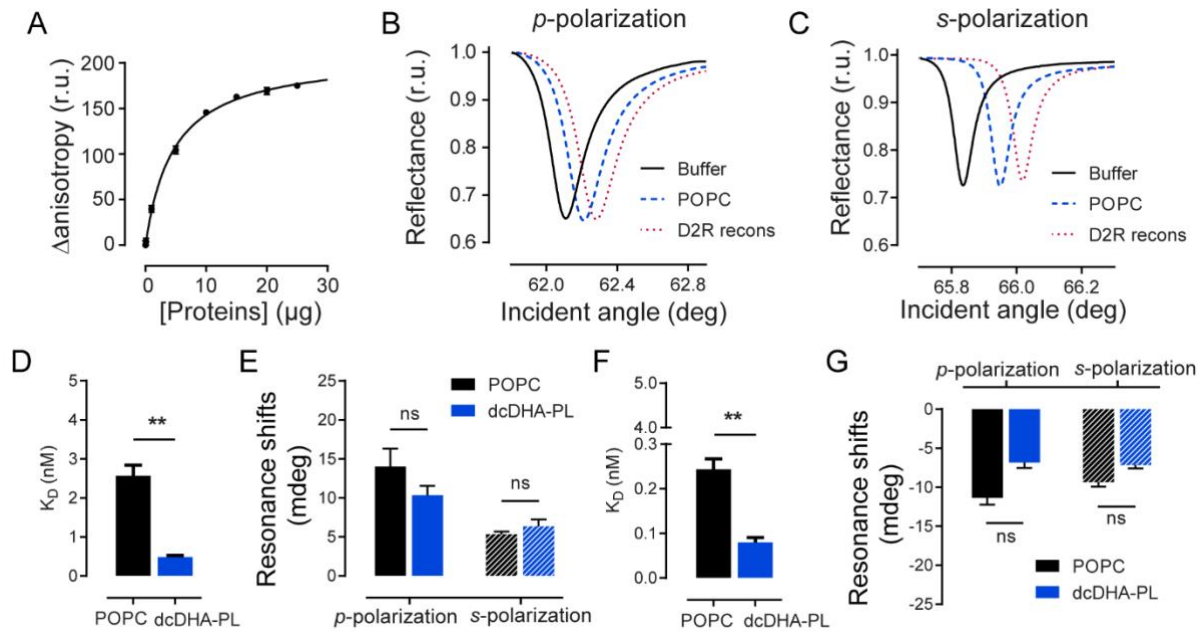
409



410

411 **Figure S4. Impact of membrane DHA on D2R ligand binding measured by fluorescence**
412 **anisotropy. (A)** Fluorescence anisotropy measurement of NAPS-d2 binding on D2R-expressing
413 membranes (total binding) or non-expressing membranes (non-specific binding). **(B)** Antagonist (NAPS-
414 d2) binding to control and DHA-enriched membranes. **(C)** Fold change of ligand affinity to D2R in DHA-
415 enriched membranes compared to control membranes. **(D)** Maximum relative binding affinity to D2R in
416 DHA-enriched membranes. Data are mean \pm SEM from three independent experiments with * $p < 0.05$
417 by two-tailed unpaired t-test.

418

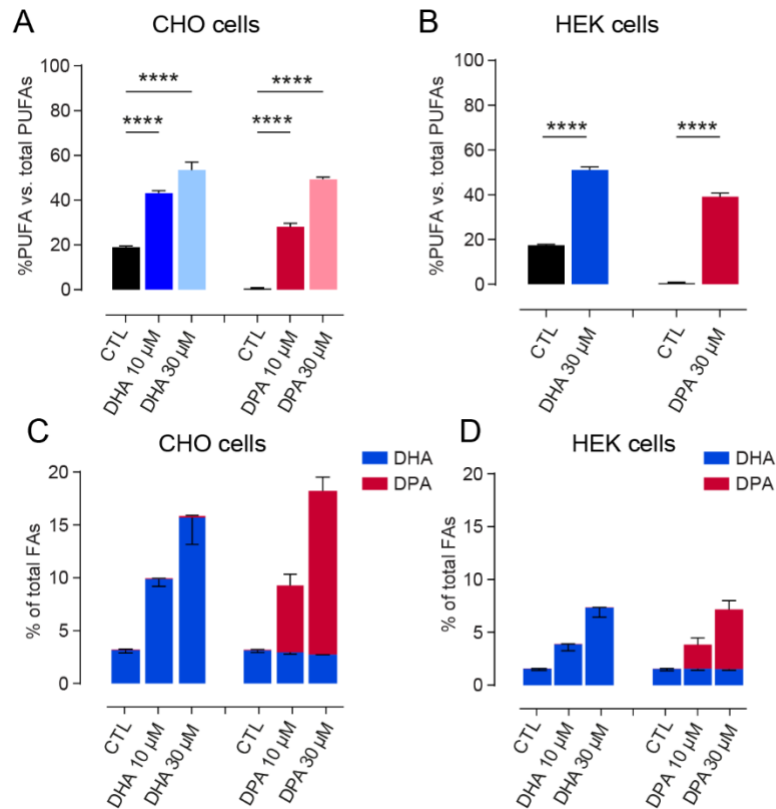


419

420

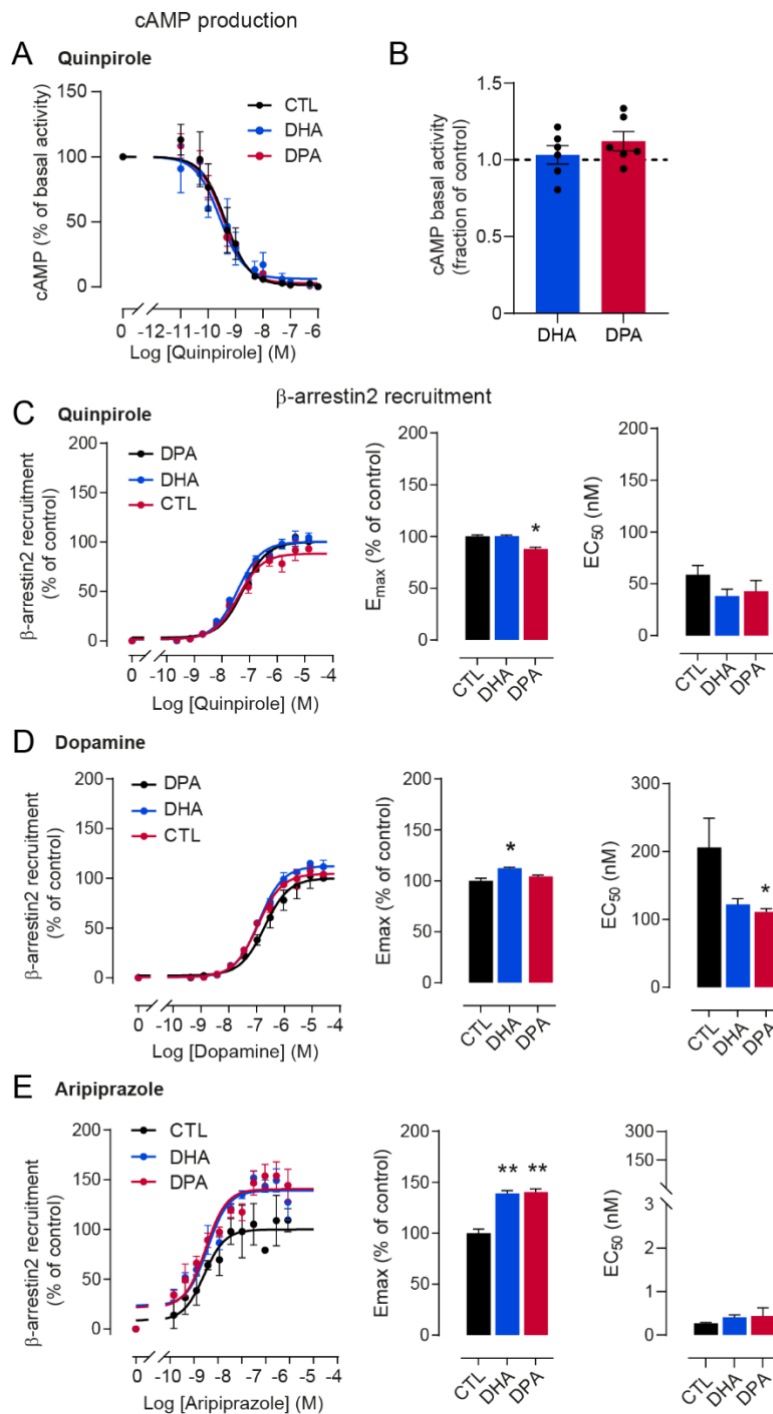
421 **Figure S5. Impact of DHA on ligand binding to D2R partially purified and reconstituted in model**
 422 **membranes shown by PWR. (A)** Fluorescence anisotropy measurement of NAPS-d2 binding to
 423 partially purified D2R (total binding). **(B and C)** Representative PWR spectra following supported POPC
 424 lipid membrane formation (blue) and D2R membrane reconstitution (red) for *p*- (B) and *s*-polarized (C)
 425 light, respectively. **(D and E)** Effect of DHA on quinpirole affinity to D2R **(D)** and quinpirole-induced
 426 receptor conformational changes **(E)** in reconstituted lipid model systems. **(F and G)** Effect of DHA on
 427 spiperone affinity to D2R **(F)** and spiperone-induced receptor conformational changes **(G)** in
 428 reconstituted lipid model systems. Data are mean \pm SEM values from at least three independent
 429 experiments with ** $p < 0.01$ by two-tailed unpaired t-test.

430



431

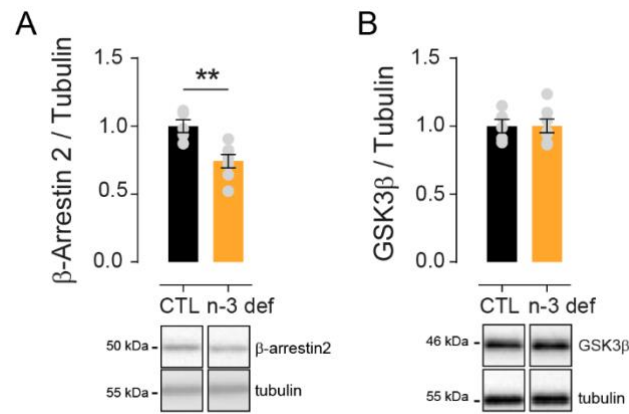
432 **Figure S6. PUFAs enrichment in CHO and HEK cells. (A)** DHA and DPA incorporation in CHO cells
433 through incubations at 10 μ M or 30 μ M. **(B)** DHA incorporation in HEK cells through incubations at 30 μ M.
434 **(C)** Cumulative PUFA incorporation in CHO cells through incubations at 10 μ M or 30 μ M. **(D)** Cumulative
435 PUFA incorporation in HEK cells through incubations at 10 μ M or 30 μ M. Bars represent the mean
436 average of three independent experiments and error bars represent the standard error of the mean
437 (SEM). ** p < 0.01, *** p < 0.001, **** p < 0.0001 by two-tailed unpaired t-test.



438

439 **Figure S7. β -arrestin2 recruitment of D2R upon stimulation by different ligands in cells**
 440 **incubated in the presence of vehicle, 10 μ M DHA or 10 μ M DPA. (A) Dose-response experiments of**
 441 **cAMP production with the D2R ligand quinpirole on forskolin-stimulated HEK cells incubated in the**
 442 **presence of 0.03% ethanol as control, 10 μ M DHA and 10 μ M DPA n-6. (B) Effect of 30 μ M PUFA**
 443 **enrichment on basal forskolin-induced cAMP production. (C) Quinpirole activity on β -arrestin2**
 444 **recruitment at the D2R in CHO-K1 cells expressing the DRD2L (left), and associated E_{max} (middle) and**
 445 **EC_{50} (right). (D) Dopamine activity on β -arrestin2 recruitment at the D2R in CHO-K1 cells expressing**
 446 **the DRD2L (left), and associated E_{max} (middle) and EC_{50} (right). (E) Aripiprazole activity on D2R**
 447 **mediated β -arrestin2 assay in CHO-K1 cells expressing the DRD2L (left), and associated E_{max} (middle)**
 448 **and EC_{50} (right). * $p < 0.05$, ** $p < 0.01$ by two-tailed unpaired t-test.**

449



450

451

452 **Figure S8. Expression of β arrestin-2 and GSK3 β in n-3 deficient mice (n-3 def). (A) and (B)**
453 Expression of β arrestin2 (A) and GSK3 β (B) by western blot normalized to the intensity of tubulin
454 expression. Bars represent the mean of five and seven subjects for CTL and n-3 def respectively and
455 error bars the SEM. ** $p < 0.01$ by Mann Whitney test.
456

	<i>CTL</i>	<i>DHA 10μM</i>	<i>DPA 10μM</i>	<i>CTL</i>	<i>DHA 30μM</i>	<i>DPA 30μM</i>
Quinpirole	9.50 \pm 0.12	9.39 \pm 0.25	9.48 \pm 0.20	9.40 \pm 0.18	9.51 \pm 0.08	9.62 \pm 0.20
Dopamine	-	-	-	8.70 \pm 0.12	8.54 \pm 0.20	8.85 \pm 0.21
Aripiprazole	-	-	-	8.08 \pm 0.25	8.36 \pm 0.16	8.46 \pm 0.10

457

458 **Table S1.** pIC₅₀ values (as mean \pm SEM) from dose-response experiments of cAMP production on
 459 forskolin-stimulated cells incubated in the presence of 0.03% ethanol as control (CTL), 10 μ M DHA and
 460 10 μ M DPA or 30 μ M DHA and 30 μ M DPA upon quinpirole, dopamine and aripiprazole stimulation of
 461 the D2R.

462

	Percentage (%)						
Model membrane	CHL1	DPPC (diC16:0)	DSPC (diC18:0)	DOPC (diC18:1)	SD(h)PC (C18:0 / C22:6)	SD(p)PC (C18:0 / C22:5)	PSM (C18:1 / C16:0)
DHA-rich	33	14	5	11	13	0	24
DPA-rich	33	14	5	11	0	13	24

463

464 **Table S2. Lipid composition of the model membranes used in MD simulations.**

465 CHL1: cholesterol, DPPC: 1,2-dipalmitoyl-sn-glycero-3-phosphocholine, DSPC: 1,2-distearoyl-sn-
 466 glycero-3-phosphocholine, DOPC: 1,2-dioleoyl-sn-glycero-3-phosphocholine, SD(h)PC: 1-stearoyl-2-
 467 docosahexaenoyl-sn-glycero-3-phosphocholine, SD(p)PC: 1-stearoyl-2- docosa(p)entaenoyl -sn-
 468 glycero-3-phosphocholine, PSM: sphingomyelin.

469

470 **Material and Methods**

471 **Chemicals and antibodies**

472 Reagents, unless otherwise specified, were from Sigma-Aldrich (St. Louis, MO, USA) PUFAs
473 (Cis-4,7,10,13,16,19-DHA (DocosaHexaenoic Acid, ref D2534), DPA n-6 (DocosaPentanoic
474 Acid, ref 18566) stock solutions (30mM) were prepared in absolute ethanol under N₂ (De
475 Smedt-Peyrusse et al., 2008). For anisotropy assays, LigandTag Lite D2 (L0002RED) receptor
476 red antagonist was purchased from Cisbio Bioassays. Quinpirole (ref 1061) and Forskolin (ref
477 1099) was from Tocris.

478

479 **Cell culture and treatment**

480 HEK 293 stably expressing the human D2R (Flp-in T-rex 293 SF-D2sWT/FRTTO 293) were
481 used. Cells were maintained at 37°C under 5% CO₂ in the following culture medium: DMEM
482 (Dulbecco's modified Eagle's medium) Glutamax (InVitroGen) containing 10% of heat
483 inactivated fetal bovine serum, 100UI/ml penicillin and 0.1mg/ml streptomycin and
484 supplemented with 100µg/ml Hygromycin (InVitrogen), 15µg/ml Blastidin (Cayla Invivogen)
485 and 1µg/ml Tetracycline (Sigma Aldrich). Upon reaching 80-90% confluence, in the same
486 culture medium, cells were treated with 10µM and 30 µM DHA or DPA or 0.03% and 0.01%
487 ethanol (vehicle) respectively as control for 24h. After treatment, cells were dissociated by
488 using an Enzyme-Free Cell Dissociation Solution (S-014-B, Merck Millipore) and washed twice
489 in wash buffer (50mM Tris-HCl, 50mM NaCl, 2mM EDTA, pH 7.5 at 20°C) by centrifugation at
490 500 × g for 8 min at 20°C. Cell pellets were used either for Western blot analyses or for
491 membrane preparation.

492

493 **Membrane preparation**

494 The cell pellets of HEK cells were resuspended in 10 ml of lysis buffer (10 mM Tris-HCl, 1 mM
495 EDTA, pH 7.5 at 4°C) supplemented with anti-protease inhibitor cocktail (PIC) (P8340, Sigma
496 Aldrich) and incubated for 30 min in ice. The cell lysate was homogenized using a 10 ml glass-
497 Teflon homogenizer with 30 gentle strokes. The resulting suspension was centrifuged at 183 ×
498 g for 10 min at 4°C. The supernatant was collected and the residual pellet was washed twice
499 by centrifugation in successively in 5 and 2.5ml of lysis buffer. The resulting supernatants were
500 pooled and centrifuged at 48000 × g for 30 min at 4°C. The pellet containing the membrane
501 proteins was resuspended in binding buffer (50 mM Tris-HCl, 50 mM NaCl, 2 mM EDTA, 2 mM
502 CaCl₂, pH 7.5 at 4°C) supplemented with PIC. Protein concentration was determined by using

503 Bicinchoninic Acid (BCA) protein assay (Uptima, Montluçon, France) and membranes were
504 diluted to 1 µg/µl in the binding buffer.

505

506 **Plasmon waveguide resonance (PWR)**

535 PWR experiments were performed with a homemade instrument equipped with a He-Ne laser
536 at 632 nm whose light is linearly polarized at 45°, allowing acquisition of both *p*- (light that is
537 parallel to the incident light) and *s*-polarization (light that is perpendicular to the incident light)
538 data within a single angular scan. The technique has been described previously^{30,69}.
539 Experiments were carried out at controlled room temperature, e.g. 23°C. The sensor consists
540 in a 90° angle prism whose hypotenuse is coated with a silver layer (50 nm) and overcoated
541 with silica (460 nm) and is in contact with the cell sample Teflon block, with an aperture of
542 approximately 3 mm diameter through which the lipid bilayer is formed. This is placed on a
543 rotating table mounted on a corresponding motion controller (Newport, Motion controller XPS;
544 ≤ 1 mdeg resolution).

545

546 **Formation of a planar lipid bilayer on the PWR sensor**

547 The method used to prepare the lipid bilayer is based on the procedure by Mueller and Rudin
548⁷⁰ to make black lipid membranes. The planar lipid bilayer is formed across the small aperture
549 (~ 3 mm) in the Teflon PWR cell by fusing freshly sonicated small unilamellar vesicles (SUV,
550 3mg/ml) with the silica surface. SUVs were prepared by initially dissolving the appropriate
551 amount of phospholipids in chloroform, to obtain the desired final concentration. A lipid film
552 was then formed by removing the solvent using a stream of N₂ (g) followed by 3h vacuum. The
553 lipid film was dispersed in PBS and thoroughly vortexed to form multi-lamellar vesicles (MLVs).
554 To form SUVs, the MLVs dispersion was sonicated 5 times during 10 minutes at 40Hz
555 frequency just before use. To ensure that a proper solid-supported lipid bilayer is formed, the
556 changes in the resonance minimum position (resulting from changes in mass density,
557 anisotropy and thickness following film deposition) for both polarizations are measured and
558 compared to values previously established to correspond to a lipid bilayer²⁵.

559

560 **Immobilisation of cell fragments on the PWR sensor**

561 The protocol for adhesion of cell fragments on silica (glass slides or PWR sensor) was adapted
562 from reported work from Perez and collaborators⁷¹. Briefly, the silica surface was washed with
563 ethanol, cleaned and activated by Plasma cleaner for 2 min (Diener, Bielefeld, Germany). The

564 silica surfaces were then incubated with a solution of poly-L-lysine (PLL, 0.1 mg/mL) for 40
565 minutes following wash with PBS buffer. Cells grown to less than 50% confluence were washed
566 with PBS and covered with water to induce osmotic swelling of the cells. Immediately, the glass
567 coverslip of the sensor was placed directly on top of cells. Pressure was applied for about 2
568 min on the glass slide or prism to induce cell rupture and caption of cell fragments. Then they
569 were removed ripping off cell fragments containing specially the upper membrane. The glass
570 slide or sensor was washed with PBS to remove cell debris and kept with buffer to prevent
571 drying and loss of membrane protein activity. PWR measurements were performed right away.
572 The PWR cell sample (volume capacity of 250 μ L) was placed in contact with the prism and
573 filled with PBS.

574

575 **Reconstitution of the dopamine D2 receptor in the lipid bilayer**

576 After lipid bilayer formation, detergent-solubilized D2 receptor was reconstituted in the lipid
577 bilayer by the detergent-dilution method. Briefly, the receptor was purified in a mixture of
578 dodecylmaltoside and cholesteryl hemisuccinate (DDM/CHS) at concentrations that are about
579 10 fold over the critical micelle concentration (cmc) of DDM. Part of the detergent was then
580 removed from the sample by use of centricons (Merck Millipore) with a cutoff of 50 KDa. This
581 consisted in concentrating and reducing the initial volume of the solubilized protein by a factor
582 of 5. The insertion of a small volume (about 20 μ L) of DDM/CHS/OG solubilized protein into
583 the PWR chamber, leads to drastic and quick drop in the detergent concentration. If the
584 detergent concentration drops below the cmc during this step, this results in immediate positive
585 PWR shifts for both *p*- and *s*-polarisations with small changes in the TIR angle. In order to
586 compare data among different experiments, data were normalized relative to the amount of
587 reconstituted protein in the membrane.

588

589 **Ligand-induced receptor response**

590 Both systems (cell fragments and reconstituted protein in lipid model systems) were tested for
591 their capacity to respond to ligand to check if the dopamine D2 receptor is active after cell
592 fragment immobilisation or reconstitution process and if it was properly reconstituted in the
593 lipid membrane. Briefly, the method consisted in incrementally adding a specific dopamine D2
594 ligand to the cell and monitor the PWR spectral changes. The first concentration point was
595 chosen to be approximately 1 order of magnitude lower than the published dissociation
596 constant (K_D) value for that ligand. Before each incremental concentration of ligand added, the
597 system was left to equilibrate. K_D values were obtained from plotting the resonance minimum

598 position of the PWR spectra (this reflects the receptor-ligand complex) as a function of total
599 ligand concentration and fitting to the hyperbolic function that describes the 1:1 binding of a
600 ligand to a receptor using GraphPad Prism (GraphPad Software).

601 A control experiment was performed that consisted in adding the same ligand concentrations
602 to a lipid bilayer with no receptor reconstituted. This measured non-specific binding of ligand
603 to lipids alone (data not shown).

604 **Fluorescence anisotropy assay**

605 Fluorescence anisotropy (FA) was used to measure receptor-ligand binding reaction into
606 individual wells of black, 96-well Greiner Bio-One microplates in a final volume of 100 μ l. To
607 establish a saturation binding curve, the range of protein membrane concentration used was
608 from 1 to 25 μ g in the presence of 10nM of the antagonist NAPS-d2 ligand (L0002 red, Cisbio
609 Bioassays). The FA was measured on a Tecan Infinite M1000 Pro microplate reader
610 (Männedorf, Switzerland). Excitation was set at 590 \pm 5 nm and emission was collected at 665
611 \pm 5 nm bandpass filters for the Texas Red.

612 The non-specific binding was obtained from membranes that did not express the receptor and
613 the total binding was measured with D2R-expressing membranes. The non-specific binding
614 curve was fitted with a Simple-linear regression in GraphPad Prism (GraphPad Software, San
615 Diego, CA), the total binding curve was fitted with a One site – total binding curve in GraphPad
616 Prism. The specific binding was determined by subtracting the non-specific curve to the total
617 binding curve and the final specific binding curve was fitted with a One site – specific binding
618 model in GraphPad Prism. The latter was used to determine relative K_D values via separated
619 saturation binding curves in at least three independent experiments and are reported as mean
620 \pm SEM.

621

622 **cAMP accumulation assays**

623 D2R stably expressing HEK 293 cells were grown on PLL treated 12-well plates as described
624 above. Upon reaching 80-90% confluence, cells were treated with 10 μ M or 30 μ M DHA or
625 DPA n-6 or 0.03 % to 0.1 % ethanol (vehicle) as control for 24 h in the culture medium. The
626 medium was removed and cells were rinsed in DMEM before pretreatment with 1mM
627 IsoButylMethylXanthine (IBMX, Sigma I5879) for 15min. Cells were then stimulated for 30min
628 with the indicated concentrations of agonists Quinpirole (Tocris 1061), Dopamine (Sigma
629 H8502) and Aripiprazole (Sigma SML0935) in the presence of 1mM IBMX and 10 μ M Forskolin
630 (Tocris 1099). Endogenous phosphodiesterase activity was stopped by removing the medium
631 and the addition of 0.1M HCL (300 μ l/well). After centrifugation at 600g during 10min, protein
632 concentration of supernatants was quantified by BCA. Cyclic AMP levels were determined in

633 samples containing 10µg of protein. The production of cAMP was measured by using a cAMP
634 Enzyme Immunoassay kit (Sigma, CA200) as described by the manufacturer using Victor3
635 (Perkin Elmer) plate reader. The curve fit was obtained by GraphPad Prism 5 (GraphPad
636 Software, Inc.).

637

638 **β-Arrestin2 recruitment assay**

639 β-arrestin2 recruitment was assessed using the PathHunter[®] express DRD2L CHO-K1 Beta
640 arrestin GCPR Assay (DiscoverX, Fremont, CA). In brief, cells were plated into 96-well white-
641 walled assay plates in a volume of 90µl of Cell Plating Reagent (DiscoverX). They were
642 incubated 24 h at 37 °C, 5 % CO₂. The next day, PUFAs (Ethanol 0.01% as control vehicle,
643 DHA, and DPA n-6) were prepared at 10X concentration (300µM) in Cell Plating Reagent and
644 10 µL was added to the cells for 24h at 37 °C, 5 % CO₂. Serial dilutions (11x) ranging from 154
645 to 0.0026 µM, 281 to 0.0046 µM and 9.35 to 0.000157 µM, of Quinpirole, Dopamine and
646 Aripiprazole respectively, were prepared and 10 µl of each concentration was added for 90
647 minutes. Luminescence was measured at 1 h post PathHunter[®] detection reagent addition
648 using Victor3 plate reader (Perkin Elmer 0.5-s/well integration time). Data were normalized to
649 control treated with the highest concentration of ligand (100%). This control value corresponds
650 to Top best fit value determined by non-linear fit of standard slope. Data were fitted to a three-
651 parameter logistic curve to generate EC₅₀ and E_{max} values (Prism, version 5.0, GraphPad
652 Software, Inc., San Diego, CA). EC₅₀ and % E_{max} values are the result of three independent
653 experiments performed in duplicate.

654 **Animals and experimental model**

655 Mice were housed in groups of 5-10 animals in standard polypropylene cages and maintained
656 in a temperature and humidity-controlled facility under a 12:12 light-dark cycle (8:00 on) with
657 ad libitum access to water and food. All animal care and experimental procedures were in
658 accordance with the INRA Quality Reference System and to french legislations (Directive
659 87/148, Ministère de l'Agriculture et de la Pêche) and European (Directive 86/609/EEC). They
660 followed ethical protocols approved by the Region Aquitaine Veterinary Services (Direction
661 Départementale de la Protection des Animaux, approval ID: B33-063-920) and by the animal
662 ethic committee of Bordeaux CEEA50. Every effort was made to minimize suffering and reduce
663 the number of animals used. C57BL/6J mouse lines from Janvier Laboratories (Robert Janvier,
664 Le Genest St-Isle France) were used in this study. Female C57BL6/J mice were fed with
665 isocaloric diets containing 5% fat with a high (n-3 def diet) or low LA/ALA ratio (Ctrl diet) across

666 gestation and lactation and offspring were maintained under the same diet after weaning as
667 previously done (see details in ¹⁴). All experiments were performed at adulthood.

668 **Operant conditioning**

669 The apparatus used for these experiments was previously described ¹⁴. Animals were food-
670 restricted in order to maintain them at 85-90% of their ad libitum weight and exposed to one
671 session (1 hour) each day, 5-7 days per week. A pavlovian training followed by fixed and
672 random ratio training were performed in order to make the animals reach an acquisition
673 criterion (i.e. the number of lever presses and rewards earned) before performing the
674 motivational task per se as previously described ¹⁴. In the motivational task, namely the
675 progressive ratio times 2 (PRx2) schedule, the number of lever presses required to earn a
676 reward was doubled respective to the previous one obtained. Mice were tested multiple times
677 in PRx2 with RR20 sessions intercalated between each PR tasks. Aripiprazole (Arip; 7-[4-[4-
678 (2,3-dichlorophenyl)piperazin-1-yl]butoxy]-3,4-dihydro-1H-quinolin-2-one; Merck®,
679 Darmstadt, Germany) was dissolved in a mixture of saline (NaCl 0.9%) and cremiphore (2%
680 of cremiphore in saline) at the doses of 0.1 and 0.5 mg/kg and administered intraperitoneally
681 10 min before the beginning of the PRx2 test sessions as previously done (Ducrocq et al., in
682 prep.). The ratio of lever presses under drugs over lever presses after vehicle injection were
683 measured for each animal and averaged in order to evaluate the effect of the drugs on operant
684 responding.

685 **Spontaneous locomotion**

686 Animals were transferred individually to small Plexiglas cages (10 cm wide, 20 cm deep, 12
687 cm tall) equipped with a video tracking system (Smart, Panlab, Barcelona, Spain) allowing the
688 recording of total distance travelled (cm) as a measure of spontaneous locomotor activity in
689 basal condition for one hour. Quinpirole-induced locomotor response was evaluated as
690 described previously (Akhisaroglu et al., 2005). Briefly, animals received 7 intraperitoneal
691 injection of 1mg/kg quinpirole (Quin ; Tocris) dissolved in 0.9% saline every 72 hours.
692 Locomotion was immediately measured for 3 hours after the 8th injection of 0.5mg/kg Quin.

693 **Western blot**

694 Mice were dislocated and the brains were quickly removed, snap-frozen on dry ice and stored.
695 Nucleus accumbens samples were punched (No.18035-01, Fine Science Tools) from 200 µm
696 frozen slices in a cryostat. Samples were homogenized and denatured and western blot were
697 performed as previously described ¹⁴. Briefly, equal quantities of proteins (10µg/well) were

698 separated by electrophoresis. Membranes were saturated and blots were probed with the
699 following primary antibodies: 1:700 rabbit anti- β Arr2 (Cell signaling Cat. No. 3857); 1:1000
700 rabbit anti-GSK3 β (Cell signaling Cat. No. 12456); 1:1000 rabbit anti-P-GSK3 β (Cell signaling
701 Cat. No. 5558); 1:10000 mouse anti-tubulin (Merck Cat. No. T5168). Then, membranes were
702 incubated with the secondary antibody coupled to Horse Radish Peroxidase (HRP, 1/5000,
703 Jackson ImmunoResearch). After revelation, optical density capture of the signal was
704 performed with the ChemidocMP imaging system (BioRad) and intensity of the signal was
705 quantified using the Image Lab software (BioRad).

706 **Cell Membrane Microarray and [³⁵S]GTP γ S autoradiography**

707 Microarrays were composed of a collection of membrane homogenates isolated from the NAc
708 of adult mice exposed to Ctrl diet (n=17) or n-3 def diet (n=17) and from rat cerebral cortex as
709 positive control. Briefly, tissue samples were homogenized using a Teflon-glass grinder
710 (Heidolph RZR 2020) and a disperser (Ultra-Turrax® T10 basic, IKA) in 20 volumes of
711 homogenized buffer (1 mM EGTA, 3 mM MgCl₂, and 50 mM Tris-HCl, pH 7.4) supplemented
712 with 250 mM sucrose. The crude homogenate was subjected to a 3,000 rpm centrifugation
713 (Allegra™ X 22R centrifuge, Beckman Coulter) for 5 min at 4°C, and the resultant supernatant
714 was centrifuged at 14,000 rpm (Microfuge® 22R centrifuge, Beckman Coulter) for 15 min (4
715 °C). The pellet was washed in 20 volumes of homogenized buffer and re-centrifuged under the
716 same conditions. The homogenate aliquots were stored at -80 °C until they were used. Protein
717 concentration was measured by the Bradford method and adjusted to the required
718 concentrations. Microarrays were fabricated by a non-contact microarrayer (Nano_plotter
719 NP2.1) placing the cell membrane homogenates (20 drops/spot) into microscope glass slides
720 treated using a proprietary technology, which enables the immobilization of cell membranes to
721 supports preserving the structure and functionality of their proteins ⁷².

722 [³⁵S]GTP γ S binding studies were carried out using Cell Membrane Microarrays according to
723 the following protocol. Briefly, Cell Membrane Microarrays were dried 20 min at room
724 temperature (r.t.), then they were incubated in assay buffer (50 mM Tris-Cl; 1 mM EGTA; 3
725 mM MgCl₂; 100 mM NaCl; 0,5% BSA; pH 7,4) in the presence or absence of 50 μ M GDP
726 and/or 100 μ M quinpirole for 15 min at r.t.. Microarrays were transferred into assay buffer
727 containing 50 μ M GDP and 0.1 nM [³⁵S]GTP γ S, with and without the dopamine D2 agonist,
728 quinpirole, at 100 μ M and incubated at 30°C for 30 min. Non-specific binding was determined
729 with GTP γ S (10 μ M). Finally, microarrays, together with [³⁵S]-standards, were exposed to films,
730 developed, scanned and quantified using the Mapix software.

731 **Lipid analyses**

732 Cells submitted to different treatments were randomly analyzed according to Joffre et al. ⁷³.
733 Total lipids were extracted according to the method developed by Folch et al. ⁷⁴ and were
734 submitted to fatty acid methylation using 7% boron trifluoride in methanol following Morrison
735 and Smith protocol ⁷⁵. Gas chromatography on a HewlettPackard Model 5890 gas
736 chromatograph (Palo Alto, CA, USA) was employed to analyze fatty acid methylesters
737 (FAMES) using aCPSIL-88 column (100 m×0.25 mm internal diameter;film thickness,0.20 µm;
738 Varian, Les Ulis, France). Hydrogen was used as a carrier gas (inlet pressure, 210 kPa). The
739 oven temperature was maintained at 60 °C for 5 min, then increased to 165 °C at 15 °C/min
740 and held for 1 min, and then to 225 °C at 2 °C/min and finally held at 225 °C for 17 min. The
741 injector and the detector were maintained at 250 °C and 280 °C, respectively. FAMES were
742 identified by comparison with commercial and synthetic standards and the data were computed
743 using the Galaxie software (Varian). The proportion of each fatty acid was expressed as a
744 percentage of total fatty acids to allow the comparison of lipid composition in different cell
745 culture conditions.

746 **MD simulations**

747 VMD1.9.4 ⁷⁶ was used to preprocess both inactive crystal (PDB ID: 6CM4) and active cryoEM
748 structures (PDB ID: 6VMS) of the dopamine D2 to set up the simulations of the apo and holo
749 states, respectively. Any co-crystallization atoms different than water molecules closer than 5
750 Å to the protein were removed. MODELLER ⁷⁷ was used to: (a) mutate back to the native
751 sequence any mutation present in the structure, namely A122I, A375L, and A379L in PDB ID:
752 6CM4, and I205T, L222R, L374M, Y378V, L381V, and I421V in PDB ID: 6VMS, and (b) model
753 residue CYS443, which is missing in the 6CM4 structure, to have the D2R palmitoylation site
754 available. The HomolWat server ⁷⁸ was used to place internal water molecules not present in
755 the initial structure, and the sodium ion in the case of apo structures. An inactive apo structure
756 was then generated by simply removing the risperidone ligand bound to PDB ID: 6CM4.
757 Likewise, an active apo structure was generated by removing the ligand bromoergocryptine
758 from PDB ID: 6VMS. This second apo structure was used to dock one molecule of either
759 dopamine or aripiprazole into the orthosteric binding pocket of the receptor using AutoDock
760 Vina ⁷⁹.

761 The CHARMM-GUI builder ^{80,81} was used to embed each refined structure were into a 90 x 90
762 Å² multicomponent membrane rich in either DHA or DPA, using a specific and realistic lipid
763 composition ²⁰, which is detailed in Table S2.

764 Each protein-membrane system was placed into a water box made of explicit water molecules,
765 their charge was neutralized, and the ionic strength of the system adjusted, throughout

766 CHARMM-GUI builder's pipeline. All titratable residues of the protein were left in their dominant
767 protonation state at pH 7.0, except for Asp80. Disulfide bridges were inserted between Cys107-
768 Cys182, and Cys399-Cys401, and a palmitoyl moiety was covalently linked to Cys443.
769 Systems were first energy minimized and then equilibrated for 50 ns at constant pressure (NPT
770 ensemble). The harmonic positional restraints initially applied to all C α atoms of the protein
771 were gradually released throughout the equilibration phase. Production simulations for each
772 replica were run for 1 μ s each, at constant volume (NVT ensemble), 1,013 bar and 310 K. The
773 production simulations of this study yielded an aggregated time of 16 μ s (4 systems x 4 replicas
774 x 1 μ s). All simulations were run using ACEMD⁸² in combination with the CHARMM36m force
775 field⁸³. Dopamine and aripiprazole ligand charges were optimized in the ANI-2x mode using
776 the parameterize module of HTMD⁸⁴. Figures from simulations were rendered using the
777 Tachyon renderer⁸⁵ and the R ggplot2 library⁸⁶.

778 Lipid-protein contact ratios between lipid species were calculated by dividing the number of
779 contacts per atom of one lipid group over the other. Atoms closer than 4.2 Å to the centre of
780 mass of the protein were considered in contact. Only lipid tail atoms were used in these
781 calculations. Each contact value was previously normalized by the total number of atoms in
782 that particular selection. For example, sn-1 SDP(d)C / SAT ratios were calculated as the
783 number of atoms of DHA < 4.2 Å of protein's centre of mass divided by the total number of
784 SDP(d)C chain atoms in the system. Likewise, SAT is calculated in the former ratio as the
785 number of atoms of any DPPC, DSPC, or PSM chain closer than 4.2 Å of protein's centre of
786 mass divided by the total number atoms of these tails.

787 The average lipid occupancy across the simulations was computed using the Python package
788 PyLipID⁸⁷.

789 **Statistical analyses**

790 Data are reported as mean \pm SEM. Statistical analyses were conducted using Prism 6 software
791 (GraphPad Software, La Jolla, CA, USA). Two-tailed unpaired Student's t-test or Mann
792 Whitney test were used to assess differences between two groups. Two-way RM ANOVA
793 followed by post-hoc Bonferroni tests were used for repeated measures. Differences were
794 considered significant for $p < 0.05$.

795

796 **References**

- 797 1. Rohrbough, J. & Broadie, K. Lipid regulation of the synaptic vesicle cycle. *Nature*
798 *Reviews Neuroscience* **6**, 139–150 (2005).
- 799 2. Bazinet, R. P. & Layé, S. Polyunsaturated fatty acids and their metabolites in brain
800 function and disease. *Nature Reviews Neuroscience* **15**, 771–785 (2014).
- 801 3. Messamore, E. & McNamara, R. K. Detection and treatment of omega-3 fatty acid
802 deficiency in psychiatric practice: Rationale and implementation. *Lipids in Health and*
803 *Disease* **15**, 1–13 (2016).
- 804 4. Gandal, M. J. *et al.* Transcriptome-wide isoform-level dysregulation in ASD,
805 schizophrenia, and bipolar disorder. *Science (80-.)*. **362**, (2018).
- 806 5. Witt, S. H. *et al.* Genome-wide association study of borderline personality disorder
807 reveals genetic overlap with bipolar disorder, major depression and schizophrenia.
808 *Transl. Psychiatry* **7**, e1155 (2017).
- 809 6. Beltz, B. S., Tlusty, M. F., Benton, J. L. & Sandeman, D. C. Omega-3 fatty acids
810 upregulate adult neurogenesis. *Neurosci. Lett.* **415**, 154–158 (2007).
- 811 7. Calderon, F. & Kim, H. Y. Docosahexaenoic acid promotes neurite growth in
812 hippocampal neurons. *J. Neurochem.* **90**, 979–988 (2004).
- 813 8. Harayama, T. & Riezman, H. Understanding the diversity of membrane lipid
814 composition. *Nat. Rev. Mol. Cell Biol.* **19**, 281–296 (2018).
- 815 9. Dawaliby, R. *et al.* Allosteric regulation of G protein-coupled receptor activity by
816 phospholipids. *Nat. Chem. Biol.* **12**, 35–39 (2016).
- 817 10. Duncan, A. L., Song, W. & Sansom, M. S. P. Lipid-dependent regulation of ion
818 channels and g protein-coupled receptors: Insights from structures and simulations.
819 *Annual Review of Pharmacology and Toxicology* **60**, 31–50 (2020).
- 820 11. Whitton, A. E., Treadway, M. T. & Pizzagalli, D. A. Reward processing dysfunction in
821 major depression, bipolar disorder and schizophrenia. *Curr. Opin. Psychiatry* **28**, 7–12
822 (2015).
- 823 12. Bondi, C. O. *et al.* Adolescent behavior and dopamine availability are uniquely
824 sensitive to dietary omega-3 fatty acid deficiency. *Biol. Psychiatry* **75**, 38–46 (2014).
- 825 13. Chalon, S. Omega-3 fatty acids and monoamine neurotransmission. *Prostaglandins*
826 *Leukot. Essent. Fat. Acids* **75**, 259–269 (2006).
- 827 14. Ducrocq, F. *et al.* Causal Link between n-3 Polyunsaturated Fatty Acid Deficiency and
828 Motivation Deficits. *Cell Metab.* **31**, 755–772 (2020).
- 829 15. Litman, B. J. & Mitchell, D. C. A role for phospholipid polyunsaturation in modulating
830 membrane protein function. *Lipids* **31**, 193–197 (1996).
- 831 16. Mitchell, D. C., Niu, S. L. & Litman, B. J. Enhancement of G protein-coupled signaling

- 832 by DHA phospholipids. *Lipids* **38**, 437–443 (2003).
- 833 17. Salem, N., Litman, B., Kim, H. & Gawrisch, K. Mechanisms of Action of
834 Docosahexaenoic Acid in the Nervous System. *Lipids* **36**, 945–959 (2001).
- 835 18. Feller, S. E., Gawrisch, K. & Woolf, T. B. Rhodopsin exhibits a preference for solvation
836 by polyunsaturated docosohexaenoic acid. *J. Am. Chem. Soc.* **125**, 4434–4435
837 (2003).
- 838 19. Pitman, M. C., Grossfield, A., Suits, F. & Feller, S. E. Role of cholesterol and
839 polyunsaturated chains in lipid-protein interactions: Molecular dynamics simulation of
840 rhodopsin in a realistic membrane environment. *J. Am. Chem. Soc.* **127**, 4576–4577
841 (2005).
- 842 20. Guixà-González, R. *et al.* Membrane omega-3 fatty acids modulate the oligomerisation
843 kinetics of adenosine A2A and dopamine D2 receptors. *Sci. Rep.* **6**, 1–13 (2016).
- 844 21. Javanainen, M. *et al.* Reduced level of docosahexaenoic acid shifts GPCR
845 neuroreceptors to less ordered membrane regions. *PLoS Comput. Biol.* **15**, 1–16
846 (2019).
- 847 22. Polozova, A. & Litman, B. J. Cholesterol dependent recruitment of di22:6-PC by a G
848 protein-coupled receptor into lateral domains. *Biophys. J.* **79**, 2632–2643 (2000).
- 849 23. Stillwell, W. & Wassall, S. R. Docosahexaenoic acid: membrane properties of a unique
850 fatty acid. *Chem. Phys. Lipids* **126**, 1–27 (2003).
- 851 24. Alves, I., Park, C. & Hruby, V. Plasmon Resonance Methods in GPCR Signaling and
852 Other Membrane Events. *Curr. Protein Pept. Sci.* **6**, 293–312 (2005).
- 853 25. Harté, E. *et al.* Probing the kinetics of lipid membrane formation and the interaction of
854 a nontoxic and a toxic amyloid with plasmon waveguide resonance. *Chem. Commun.*
855 **50**, 4168–4171 (2014).
- 856 26. De Jong, L. A. A., Grünewald, S., Franke, J. P., Uges, D. R. A. & Bischoff, R.
857 Purification and characterization of the recombinant human dopamine D2S receptor
858 from *Pichia pastoris*. *Protein Expr. Purif.* **33**, 176–184 (2004).
- 859 27. Malmberg, A. & Mohell, N. Characterization of [3H]quinpirole binding to human
860 dopamine D(2A) and D3 receptors: Effects of ions and guanine nucleotides. *J.*
861 *Pharmacol. Exp. Ther.* **274**, 790–797 (1995).
- 862 28. Albizu, L. *et al.* Time-resolved FRET between GPCR ligands reveals oligomers in
863 native tissues. *Nat. Chem. Biol.* **6**, 587–594 (2010).
- 864 29. Maurel, D. *et al.* Cell-surface protein-protein interaction analysis with time-resolved
865 FRET and snap-tag technologies: Application to GPCR oligomerization. *Nat. Methods*
866 **5**, 561–567 (2008).
- 867 30. Alves, I. D. & Lecomte, S. Study of G-Protein Coupled Receptor Signaling in
868 Membrane Environment by Plasmon Waveguide Resonance. *Acc. Chem. Res.* **52**,

- 869 1059–1067 (2019).
- 870 31. Alves, I. D. *et al.* Different structural states of the proteolipid membrane are produced
871 by ligand binding to the human δ -opioid receptor as shown by plasmon-waveguide
872 resonance spectroscopy. *Mol. Pharmacol.* **69**, 406 (2004).
- 873 32. Alves, I. D. *et al.* The two NK-1 binding sites correspond to distinct, independent, and
874 non-interconvertible receptor conformational states as confirmed by plasmon-
875 waveguide resonance spectroscopy. *Biochemistry* **45**, 5309–5318 (2006).
- 876 33. Boyé, K. *et al.* The role of CXCR3/LRP1 cross-talk in the invasion of primary brain
877 tumors. *Nat. Commun.* **8**, 1–20 (2017).
- 878 34. Boyé, K., Billottet, C., Pujol, N., Alves, I. D. & Bikfalvi, A. Ligand activation induces
879 different conformational changes in CXCR3 receptor isoforms as evidenced by
880 plasmon waveguide resonance (PWR). *Sci. Rep.* **7**, 1–11 (2017).
- 881 35. Guixà-González, R. *et al.* Membrane cholesterol access into a G-protein-coupled
882 receptor. *Nat. Commun.* 2017 81 **8**, 1–12 (2017).
- 883 36. Beaulieu, J. M., Gainetdinov, R. R. & Caron, M. G. The Akt-GSK-3 signaling cascade
884 in the actions of dopamine. *Trends in Pharmacological Sciences* **28**, 166–172 (2007).
- 885 37. Lafourcade, M. *et al.* Nutritional omega-3 deficiency abolishes endocannabinoid-
886 mediated neuronal functions. *Nat. Neurosci.* **14**, 345–350 (2011).
- 887 38. Mizumura, T. *et al.* Activation of adenosine A2A receptor by lipids from
888 docosahexaenoic acid revealed by NMR. *Sci. Adv.* **6**, 8544–8562 (2020).
- 889 39. Carrillo-Tripp, M. & Feller, S. E. Evidence for a mechanism by which ω -3
890 polyunsaturated lipids may affect membrane protein function. *Biochemistry* **44**, 10164–
891 10169 (2005).
- 892 40. Bruno, M. J., Koeppe, R. E. & Andersen, O. S. Docosahexaenoic acid alters bilayer
893 elastic properties. *Proc. Natl. Acad. Sci. U. S. A.* **104**, 9638–9643 (2007).
- 894 41. Caires, R. *et al.* Omega-3 Fatty Acids Modulate TRPV4 Function through Plasma
895 Membrane Remodeling. *Cell Rep.* **21**, 246–258 (2017).
- 896 42. Antonny, B., Vanni, S., Shindou, H. & Ferreira, T. From zero to six double bonds:
897 Phospholipid unsaturation and organelle function. *Trends in Cell Biology* **25**, 427–436
898 (2015).
- 899 43. Gawrisch, K., Eldho, N. V. & Holte, L. L. The structure of DHA in phospholipid
900 membranes. *Lipids* **38**, 445–452 (2003).
- 901 44. Jacobs, M. L., Faizi, H. A., Peruzzi, J. A., Vlahovska, P. M. & Kamat, N. P. EPA and
902 DHA differentially modulate membrane elasticity in the presence of cholesterol.
903 *Biophys. J.* **120**, 2317–2329 (2021).
- 904 45. Alves, I., Staneva, G., Tessier, C., Salgado, G. F. & Nuss, P. The interaction of
905 antipsychotic drugs with lipids and subsequent lipid reorganization investigated using

- 906 biophysical methods. *Biochim. Biophys. Acta - Biomembr.* **1808**, 2009–2018 (2011).
- 907 46. Tessier, C., Nuss, P., Staneva, G. & Wolf, C. Modification of membrane heterogeneity
908 by antipsychotic drugs: An X-ray diffraction comparative study. *J. Colloid Interface Sci.*
909 **320**, 469–475 (2008).
- 910 47. Lolicato, F. *et al.* Membrane-Dependent Binding and Entry Mechanism of Dopamine
911 into Its Receptor. *ACS Chem. Neurosci.* **11**, 1914–1924 (2020).
- 912 48. Grossfield, A., Feller, S. E. & Pitman, M. C. A role for interactions in the modulation of
913 rhodopsin by ω -3 polyunsaturated lipids. *Proc. Natl. Acad. Sci. U. S. A.* **103**, 4888–
914 4893 (2006).
- 915 49. Soubias, O., Teague, W. E. & Gawrisch, K. Evidence for specificity in lipid-rhodopsin
916 interactions. *J. Biol. Chem.* **281**, 33233–33241 (2006).
- 917 50. Lemel, L. *et al.* The ligand-bound state of a G protein-coupled receptor stabilizes the
918 interaction of functional cholesterol molecules. *J. Lipid Res.* **62**, 100059 (2021).
- 919 51. Malnoe, A., Milon, H. & Reme, C. Effect of In Vivo Modulation of Membrane
920 Docosahexaenoic Acid Levels on the Dopamine-Dependent Adenylate Cyclase
921 Activity in the Rat Retina. *J. Neurochem.* **55**, 1480–1485 (1990).
- 922 52. Murphy, M. G. Effects of exogenous linoleic acid on fatty acid composition, receptor-
923 mediated cAMP formation, and transport functions in rat astrocytes in primary culture.
924 *Neurochem. Res.* **20**, 1365–1375 (1995).
- 925 53. Yu, J. Z., Wang, J., Sheridan, S. D., Perlis, R. H. & Rasenick, M. M. N-3
926 polyunsaturated fatty acids promote astrocyte differentiation and neurotrophin
927 production independent of cAMP in patient-derived neural stem cells. *Mol. Psychiatry*
928 (2020). doi:10.1038/s41380-020-0786-5
- 929 54. Chapkin, R. S., Wang, N., Fan, Y. Y., Lupton, J. R. & Prior, I. A. Docosahexaenoic
930 acid alters the size and distribution of cell surface microdomains. *Biochim. Biophys.*
931 *Acta - Biomembr.* **1778**, 466–471 (2008).
- 932 55. Levental, K. R. *et al.* Polyunsaturated Lipids Regulate Membrane Domain Stability by
933 Tuning Membrane Order. *Biophys. J.* **110**, 1800–1810 (2016).
- 934 56. Stillwell, W., Shaikh, S. R., Zerouga, M., Siddiqui, R. & Wassal, S. R.
935 Docosahexaenoic acid affects cell signaling by altering lipid rafts. *Reproduction*
936 *Nutrition Development* **45**, 559–579 (2005).
- 937 57. Charest, P. G. & Bouvier, M. Palmitoylation of the V2 Vasopressin Receptor Carboxyl
938 Tail Enhances β -Arrestin Recruitment Leading to Efficient Receptor Endocytosis and
939 ERK1/2 Activation. *J. Biol. Chem.* **278**, 41541–41551 (2003).
- 940 58. Hawtin, S. R., Tobin, A. B., Patel, S. & Wheatley, M. Palmitoylation of the Vasopressin
941 V1a Receptor Reveals Different Conformational Requirements for Signaling, Agonist-
942 induced Receptor Phosphorylation, and Sequestration. *J. Biol. Chem.* **276**, 38139–

- 943 38146 (2001).
- 944 59. Karnik, S. S., Ridge, K. D., Bhattacharya, S. & Khorana, H. G. Palmitoylation of bovine
945 opsin and its cysteine mutants in COS cells. *Proc. Natl. Acad. Sci. U. S. A.* **90**, 40–44
946 (1993).
- 947 60. Moffett, S., Mouillac, B., Bonin, H. & Bouvier, M. Altered phosphorylation and
948 desensitization patterns of a human β 2-adrenergic receptor lacking the palmitoylated
949 Cys341. *EMBO J.* **12**, 349–356 (1993).
- 950 61. Palmer, T. M. & Stiles, G. L. Identification of threonine residues controlling the agonist-
951 dependent phosphorylation and desensitization of the rat A3 adenosine receptor. *Mol.*
952 *Pharmacol.* **57**, 539–545 (2000).
- 953 62. Pickering, D. S., Taverna, F. A., Salter, M. W. & Hampson, D. R. Palmitoylation of the
954 GluR6 kainate receptor. *Proc. Natl. Acad. Sci. U. S. A.* **92**, 12090–12094 (1995).
- 955 63. Lally, C. C. M., Bauer, B., Selent, J. & Sommer, M. E. C-edge loops of arrestin
956 function as a membrane anchor. *Nat. Commun.* **8**, 1–12 (2017).
- 957 64. Donthamsetti, P. *et al.* Arrestin recruitment to dopamine D2 receptor mediates
958 locomotion but not incentive motivation. *Mol. Psychiatry* **25**, 2086–2100 (2020).
- 959 65. Gallo, E. F. *et al.* Accumbens dopamine D2 receptors increase motivation by
960 decreasing inhibitory transmission to the ventral pallidum. *Nat. Commun.* **9**, 1–13
961 (2018).
- 962 66. Berger, G. E. *et al.* Ethyl-Eicosapentaenoic Acid in First-Episode Psychosis: A
963 Randomized, Placebo-Controlled Trial. *J. Clin. Psychiatry* **68**, 1867–75 (2007).
- 964 67. Robinson, D. G. *et al.* A potential role for adjunctive omega-3 polyunsaturated fatty
965 acids for depression and anxiety symptoms in recent onset psychosis: Results from a
966 16 week randomized placebo-controlled trial for participants concurrently treated with
967 risperidone. *Schizophr. Res.* **204**, 295–303 (2019).
- 968 68. Amminger, G. P., Schäfer, M. R., Schlögelhofer, M., Klier, C. M. & McGorry, P. D.
969 Longer-term outcome in the prevention of psychotic disorders by the Vienna omega-3
970 study. *Nat. Commun.* **2015 61 6**, 1–7 (2015).
- 971 69. Salamon, Z., Macleod, H. A. & Tollin, G. Coupled plasmon-waveguide resonators: A
972 new spectroscopic tool for probing proteolipid film structure and properties. *Biophys. J.*
973 **73**, 2791–2797 (1997).
- 974 70. Mueller, P. & Rudin, D. O. Resting and action potentials in experimental bimolecular
975 lipid membranes. *J. Theor. Biol.* **18**, 222–258 (1968).
- 976 71. Perez, J. B. *et al.* Monitoring the Diffusion of Single Heterotrimeric G Proteins in
977 Supported Cell-membrane Sheets Reveals their Partitioning into Microdomains. *J.*
978 *Mol. Biol.* **363**, 918–930 (2006).
- 979 72. Fernández, R. *et al.* Microarray and Mass Spectrometry-Based Methodology for Lipid

- 980 Profiling of Tissues and Cell Cultures. *Anal. Chem.* **91**, 15967–15973 (2019).
- 981 73. Joffre, C. *et al.* Modulation of brain PUFA content in different experimental models of
982 mice. *Prostaglandins Leukot. Essent. Fat. Acids* **114**, 1–10 (2016).
- 983 74. Folch, J., Lees, M. & Sloane Stanley, G. H. A simple method for the isolation and
984 purification of total lipides from animal tissues. *J. Biol. Chem.* **226**, 497–509 (1957).
- 985 75. Morrison, W. R. & Smith, L. M. Preparation of fatty acid methyl esters and
986 dimethylacetals from lipids. *J. Lipid Res.* **5**, 600–608 (1964).
- 987 76. Humphrey, W., Dalke, A. & Schulten, K. VMD: Visual molecular dynamics. *J. Mol.*
988 *Graph.* **14**, 33–38 (1996).
- 989 77. Webb, B. & Sali, A. Comparative protein structure modeling using MODELLER. *Curr.*
990 *Protoc. Bioinforma.* **2016**, 5.6.1-5.6.37 (2016).
- 991 78. Mayol, E. *et al.* Homolwat: A web server tool to incorporate ‘homologous’ water
992 molecules into gpcr structures. *Nucleic Acids Res.* **48**, W54–W59 (2020).
- 993 79. Trott, O. & Olson, A. J. AutoDock Vina: Improving the speed and accuracy of docking
994 with a new scoring function, efficient optimization, and multithreading. *J. Comput.*
995 *Chem.* **31**, (2009).
- 996 80. Jo, S., Kim, T. & Im, W. Automated builder and database of protein/membrane
997 complexes for molecular dynamics simulations. *PLoS One* **2**, e880 (2007).
- 998 81. Wu, E. L. *et al.* CHARMM-GUI membrane builder toward realistic biological membrane
999 simulations. *Journal of Computational Chemistry* **35**, 1997–2004 (2014).
- 1000 82. Harvey, M. J., Giupponi, G. & De Fabritiis, G. ACEMD: Accelerating biomolecular
1001 dynamics in the microsecond time scale. *J. Chem. Theory Comput.* **5**, 1632–1639
1002 (2009).
- 1003 83. Huang, J. *et al.* CHARMM36m: An improved force field for folded and intrinsically
1004 disordered proteins. *Nat. Methods* **14**, 71–73 (2016).
- 1005 84. Doerr, S., Harvey, M. J., Noé, F. & De Fabritiis, G. HTMD: High-Throughput Molecular
1006 Dynamics for Molecular Discovery. *J. Chem. Theory Comput.* **12**, 1845–1852 (2016).
- 1007 85. Stone, J. E., Vandivort, K. L. & Schulten, K. GPU-accelerated molecular visualization
1008 on petascale supercomputing platforms. in *Proc. of UltraVis 2013: 8th Int. Workshop*
1009 *on Ultrascale Visualization - Held in Conjunction with SC 2013: The Int. Conference*
1010 *for High Performance Computing, Networking, Storage and Analysis* (2013).
1011 doi:10.1145/2535571.2535595
- 1012 86. Wickham, H. Ggplot2: Elegant Graphics for Data Analysis. in *Springer* (2016).
- 1013 87. Song, W. *et al.* Pylipid: A Python Toolkit for Analysis of Lipid-Protein Interactions from
1014 MD Simulations. *bioRxiv* **120**, 48a (2021).
- 1015
- 1016

1017

1018 **Acknowledgements**

1019 We thank the biochemistry facility of the Bordeaux Neurocampus for the access to the blot
1020 imaging system, JP. Toulmé for use of the fluorescence spectrometer (TECAN), JL Banere for
1021 providing D2R expressing *Pichia pastoris* and the Bordeaux Metabolome Facility-MetaboHUB
1022 (ANR-11-INBS-0010).

1023 This study was supported by INRAE, CNRS and the University of Bordeaux, Idex
1024 Bordeaux “chaire d’installation” (ANR-10-IDEX-03-02) (P.T.), NARSAD Young Investigator
1025 Grants from the Brain and Behavior Foundation (P.T.), ANR “SynLip” (ANR-16-CE16-0022)
1026 (P.T.), ANR “FrontoFat” (ANR-20-CE14-0020) (P.T.), Region Nouvelle Aquitaine 2014-
1027 1R30301-00003023 (P.T.), NIH grant MH54137 (J.A.J), the Instituto de Salud Carlos III
1028 FEDER (PI18/00094) and the ERA-NET NEURON & Ministry of Economy, Industry and
1029 Competitiveness (AC18/00030) (J.S.), the European Research Network on Signal
1030 Transduction (<https://ernest-gpcr.eu>) (COST Action CA18133) (B.M., R.G-G., J.S.), the Swiss
1031 National Science Foundation, grant no. 192780 (R.G-G.).

1032

1033

1034 **Author contributions**

1035 M-L.J, V.D.P, R.G-G, I.D.A. and P.T. conceived and supervised the study. J.S., G.B-G., E.M.,
1036 T.D. and J.A.J. provided expertise, reagents and supervised specific experiments. M-L.J.,
1037 V.D.P., F.D., A.O., R.B., M.H.P., B.M-L., J.S., S.M., T.T-C., S.G. and R.G-G performed
1038 experiments and analyzed the data. M-L.J., V.D.P., R.G.-G., I.D.A. and P.T. wrote the original
1039 version of the manuscript. All authors discussed the results and reviewed the manuscript.

1040

1041 **Competing financial interest**

1042 The authors declare no competing interests.